Ammonia adsorptive capture and Sequential Phosphorus Recovery as two nutrient products from anaerobic membrane bioreactor (AnMBR) swine permeate

by

Nicholas McKee-Rist

B.S., Kansas State University, 2022

A THESIS

submitted in partial fulfillment of the requirements for the degree

MASTER OF SCIENCE

Department of Civil Engineering
Cark R. Ice College of Engineering

KANSAS STATE UNIVERSITY
Manhattan, Kansas

2025

Approved by:

Major Professor
Dr. Prathap Parameswaran

Copyright

Abstract

Managing swine wastewater presents environmental challenges and resource recovery opportunities within a circular economy framework. Phosphorus is an essential nutrient for agricultural productivity, yet its primary source, phosphate rock, is a finite resource. Swine wastewater, a byproduct of concentrated animal feeding operations (CAFOs), contains high concentrations of phosphorus (P) and nitrogen (N), which contribute to eutrophication and greenhouse gas emissions if not adequately managed. This study explores the potential for nutrient recovery from swine wastewater using a combination of physicochemical processes to sequester phosphorus and ammonia in reusable forms. Specifically, anaerobic treatment systems, including Anaerobic Membrane Bioreactors (AnMBRs), were employed to facilitate microbial fermentation and selective nutrient capture, with a focus on optimizing the production of recoverable phosphorus precipitates and ammonia-based fertilizers.

The sequential recovery process involved pH adjustment to 4.5 using hydrochloric acid (HCl) to strip bicarbonate ions, followed by the addition of calcium oxide (CaO) and magnesium chloride ($MgCl_2$) to precipitate phosphorus. Two chemical addition sequences were tested: CaO followed by $MgCl_2$ and $MgCl_2$ followed by CaO. The CaO-first sequence at a 0.5:1 Ca:P molar ratio, followed by $MgCl_2$ at a 1:1 Mg:P ratio, demonstrated the highest phosphorus removal efficiency (89.60% after 7 hours) and favored the formation of amorphous calcium phosphate (ACP), a highly soluble quick-release fertilizer. Struvite formation was also observed at lower Ca ratios, indicating the potential for producing mixed fertilizers with varying nutrient release rates. Controlled pH conditions (7-9) were critical for enhancing phosphorus precipitation, while high alkalinity led to unwanted calcium carbonate ($CaCO_3$) formation, reducing the fertilizer value of the product.

In addition to phosphorus recovery, ammonia capture on clinoptilolite was evaluated as a precursor to liquid fertilizer production, with adsorption capacities influenced by influent concentration and contact time.

The findings highlight the importance of optimizing chemical addition sequences, reaction times, and pH conditions to maximize nutrient recovery and produce high-quality fertilizer products. This research provides a framework for integrating phosphorus and nitrogen recovery into agricultural and municipal wastewater treatment systems, reducing reliance on mined phosphate, and promoting sustainable nutrient management. By recovering valuable nutrients from swine wastewater, this study contributes to the development of circular nutrient use, enhancing fertilizer production from waste streams, and mitigating the environmental risks associated with nutrient-laden agricultural runoff. The integration of these technologies underscores the potential for decentralized wastewater treatment systems to contribute to sustainable agriculture and environmental stewardship.

Table of Contents

List of Figures

List of Tables

Acknowledgements

This work was supported by the U.S. Department of Energy (DoE-DEEE00009504). Their continued investment in research and innovation is essential to scientific advancements. Another acknowledgment is due to the Kansas Game-Changing Research Initiative Program (KGRIP) for supporting innovative solutions that drive progress towards a more sustainable food system

I want to start by expressing my utmost gratitude to Dr. Prathap Parameswaran for giving me this opportunity to be under his wing. Coming from a mechanical engineering background, I had much to learn in the field of wastewater. I sincerely appreciate the time and effort he dedicated to passing down his knowledge and sharing his passion for innovative treatment technologies. His mentorship has been invaluable throughout this journey.

Would also like to thank Dr. Ganga Hettiarachchi for taking the time to help me understand the broader implications of the products developed in our lab. Through her insights on soil health and the benefits of sustainable fertilizers, I connected my research to its real-world environmental impact. Her perspective helped me fully appreciate the potential of our work to contribute to more sustainable agricultural practices.

I would also like to thank Dr. Arvind Damodara Kannan and Jaime Herrera for laying the foundation for this research. Their prior work served as the backbone of this project, providing the framework I could build and expand on. I am deeply appreciative of their contributions, which enabled the progress of this study.

A big thank you to everyone who supported me in the lab throughout this journey. From teaching me how to operate the Hach spectrophotometer to assisting with analyses, your help was invaluable. I am especially grateful to Jack Dillavou, Lucas Hopper, Elinor Steinbach, Chinmay Deore, Skype Palar, Jordan Williams, Caitlin Swope, and Mason Ericson—along with

many others who came and went during the course of this work. Your contributions, whether big or small, made this experience all the more meaningful. Also thank you to Dr. Kasuni Haputhanthri Gammage and Jack Murphy for your time freeze drying and analyzing all the solids from our Phosphorus trials with XRD. This information was invaluable in helping strengthening the research.

A special thank you goes out to Brooke Vogt for her instrumental role in developing both the procedure used in the sequential phosphorus recovery experiments (Chapters 3 and 4) and the extremely useful Excel template that streamlined our work. Her contributions helped keep our data organized, ensured proper dosing calculations, and provided an all-in-one tool that proved invaluable throughout the research process.

A thank you is also owed to generative AI tools like ChatGPT and Grammarly. As a student who struggles with dyslexia, these tools have been incredibly helpful in refining my writing and improving clarity throughout the course of this work. Their support made the writing process more accessible and manageable.

I would also like to acknowledge Parnian Mohammadiansemnani for her current contributions and future work on this project. It has been a pleasure introducing her to the nutrient recovery system and sharing what I've learned along the way. I'm excited to see how her research will continue to advance and shape the next phase of this work.

I would also like to thank environmental scientist and degrowth author Dr. Kohei Saito. His writings have inspired me to think more critically about the role of sustainability, resource recovery, and environmental justice in scientific research. His work continues to shape my perspective on the broader purpose of what we do in the lab.

Lastly, I would like to thank all my friends who gave me much-needed breaks from research, whether it was playing video games like Dota, going out to the bars, or just hanging out and talking. The moments shared in these social circles, especially with YDSA and Delta Chi, have been incredibly meaningful. I'll always value the support, laughter, and camaraderie that helped keep me grounded throughout this journey.

Dedication

This paper is dedicated to my loving family. To my parents—thank you for always encouraging me to pursue my interests, from joining robotics to attending Science City. Without your unwavering support from the very beginning, I may never have found the path that led me here.

A heartfelt thank you also goes to my grandparents, both living and passed, who always believed in me and offered their love and wisdom throughout my life.

And lastly, to my caring girlfriend, thank you for standing by my side throughout my entire master's program. From studying together to helping me grasp chemistry concepts I lacked coming in, your constant support has meant the world to me.

Thank you all for helping me become the man I am today.

Chapter 1 - Background and Literature Review

1.1 Impacts of industrial agriculture and CAFOs

Industrial agriculture and concentrated animal feeding operations (CAFOs) have become cornerstones of global food production since the 1950s (Thu & Durrenberger, 2000). While these systems have improved food production efficiency, they have also introduced significant environmental challenges, particularly water quality degradation due to nutrient pollution.

Each year, the U.S. produces 335 million tons of manure from concentrated animal feeding operations (CAFOs), surpassing the amount that croplands can sustainably absorb. (https://www.epa.gov/nps/nonpoint-source-agriculture and USDA Manure Management for water quality). In regions such as North Carolina's Coastal Plain and the Midwest Corn Belt, CAFOs produce vast quantities of animal waste rich in nitrogen (N) and phosphorus (P) that often surpass the assimilative capacity of the local landscape. While manure is commonly used as fertilizer, its excessive and poorly managed application leads to the runoff and leaching of nutrients into surrounding surface and groundwater systems (Mallin & Cahoon, 2003). This is further compounded by manure's nitrogen-to-phosphorus (N:P) ratio. When manure is applied according to the nitrogen requirements of crops, it often leads to the overapplication of phosphorus, which contributes to the buildup of excess P in amended soils and heightens the risk of phosphorus loss to nearby water bodies. (Bian, 2021)

Agricultural nutrient runoff is the leading cause of water quality impairment in U.S. rivers and streams, as well as third for lakes (EPA). Excess nitrogen and phosphorus entering freshwater systems promote the overgrowth of algae, a phenomenon known as eutrophication. When algal blooms die off, their decomposition depletes oxygen, creating hypoxia "dead zones" that cannot support aquatic life. This impact is localized and moves downstream, affecting larger

bodies of water. Scientists have observed an “dead zone” annually occurring in the Gulf of Mexico for over three decades. In this area, oxygen levels are reduced so low that most marine life cannot survive. Sixty to eighty percent of the nitrogen contributing to this dead zone originates from agricultural and livestock operations in the Midwest (Boehm 2022). Another equally important negative impact of current CAFO manure and waste management practices (land application, lagoons) is the emission of greenhouse gases, namely methane, nitrous oxide, Carbon dioxide, and others such as ammonia. The odor emissions from CAFO waste lagoons continue to create socio-economic constraints in rural and agriculturally intensive production zones such as the Midwest and mid-Atlantic states in the US .

These environmental impacts cascade into economic and social consequences. Hypoxia undermines commercial and recreational fisheries, affecting thousands of jobs and billions in economic activity across the Gulf Coast. Simultaneously, upstream communities face degraded drinking water supplies and diminished ecosystem services. Studies estimate that nitrogen runoff has caused up to $2.4 billion in damages yearly since the 1980s, affecting the ecosystem services generated by fisheries and marine habitats. (Boehm 2022).

Current animal waste management at CAFOs relies heavily on traditional methods, prioritizing containment over recovery. The most widespread approach is direct land application of manure, which, while beneficial as a soil amendment, frequently leads to nutrient overloading when applied in excess of crop needs. Other common strategies include open anaerobic lagoons that allow for long-term storage and partial waste degradation, although they are prone to emissions and leakage. Covered anaerobic lagoons, by contrast, offer some control over greenhouse gas emissions and enable biogas capture. In more confined animal housing systems, deep manure storage pits are used to collect waste beneath barns. A small but growing number of

operations have also adopted anaerobic digestion reactors, which facilitate enhanced organic matter breakdown and energy recovery. However, these systems remain limited due to cost, maintenance requirements, and technical expertise. As a result, most CAFOs continue to rely on land application as the primary waste disposal method, with limited implementation of nutrient recovery technologies.

This has enabled emerging technologies to provide pathways for cleaning and transforming waste into valuable resources. Recovering N and P from agricultural wastewater could mitigate eutrophication risks while generating economic returns. For instance, anaerobic digestion systems capture methane from manure for energy production, and struvite precipitation recovers phosphorus as a slow-release fertilizer (Sharrer et al., 2020). Such processes align with circular economy principles, reducing reliance on synthetic fertilizers and fossil fuels (Ellen MacArthur Foundation, 2019). However, high capital costs and maintenance cost with its complex infrastructure requirements contribute to the continued lag in widespread adoption (Sharrer et al., 2020; Ellen MacArthur Foundation, 2019). As a result, most CAFO-generated waste continues to be land-applied with minimal treatment, perpetuating the cycle of nutrient overloading and environmental degradation.

1.2 Need for nutrient recovery from swine CAFO waste

Even though N is the most abundant element in the earth's atmosphere, its availability as a synthetic ammonia fertilizer has largely been reliant upon the Haber Bosch process (Mulder, 2003). The Haber Bosch process involves energy intensive ammonia generation (~10 kWh/kg N) process that consumes 1.8% of global energy output each year and consequently produces approximately 500 million tons of carbon dioxide, equating to about 1.8% of global carbon dioxide emissions. (Maurer et al., 2003; Razon, 2014).

An equally important nutrient to sustain plant life is P, a non-renewable resource extensively used as a fertilizer (Azam, 2019). The main source of P is from the mining of phosphate rock. While there have been concerns about possible depletion of all phosphorus reserves, it is currently speculated that reserves are sufficient for well over a millennium when accounting for lower grade ore deposits. However, this mining of lower-grade ores will come at the cost of higher water and energy use (Wellmer, 2023). It is expected that by 2060 there will be an increase of 40% for using phosphorus fertilizers (Scholz, 2025). With an estimated emission factor to produce P fertilizers of around 0.54 tons CO2 per ton P2O5.(Walling,2020), there is a need to recover and reuse both ammonia and.

With the increasing amount of nutrient-rich wastewaters generated from different sources, including municipal, agricultural, and industrial wastewaters such as swine, poultry, dairy, wool scours, abattoirs, human urine, sewage, tanneries, etc. (Kumar & Pal, 2015; Saliu & Oladoja, 2021), closed-loop phosphorus recovery in agriculture and industry could reduce mining dependency by 30–50% (Bai, 2024; Scholz, 2025). The choice of the resource recovery platform is dictated by the concentrations of nutrients (N and P) and organic carbon in the wastewaters, which could vary widely depending on the type or source of wastewater.

1.3 Nutrient Recovery Techniques

1.3.1 Chemical Precipitation for phosphorus

Chemical precipitation is a widely used method for removing nutrients from wastewater, particularly phosphorus and nitrogen, to enable compliance with discharge requirements, with some recent efforts to turn them into valuable fertilizer products. Chemical phosphorus removal pertains to mainstream wastewater treatment. At the same time, nutrient recovery technologies have been focused on side stream treatment from anaerobic digester centrate to reduce

headworks nutrients return load while producing beneficial products. Two significant recovered nutrient products of significance in municipal wastewater treatment of this process are struvite ($MgNH_4PO_4 \cdot 6H_2O$) and calcium phosphate, both recognized for their effectiveness as slow-release fertilizers in agriculture. There are several commercial efforts to scale up nutrient recovery as struvite or Calcium phosphate at different levels of market readiness

Recovery Method	Recovery Type	Company / Developer	Technology Readiness Level
Struvite Precipitation	Chemical precipitation	Ostara (Pearl),	Full-scale
Struvite Precipitation	Chemical precipitation	NuReSys	R&D
Struvite Precipitation	Chemical precipitation	MagPrex CNP	Estabished
Calcium Phosphate (CaP)	Chemical precipitation	CalPrex (CentriSys)	Pilot- R&D

Table 1.1: Commercial technologies for struvite and calcium phosphate recovery

Struvite is formed by adding magnesium salts such as MgO, $MgCl_2$, or $Mg(OH)_2$, which react with ammonium (NH_4^+) and phosphate (PO_4^{3-}) present in the wastewater to create a crystalline compound (Stolzenburg et al., 2015). Magnesium often serves as the limiting ion in this process, making its addition essential for successful precipitation. Several operational factors influence struvite formation, including pH, temperature, phosphate concentration, and the presence of competing ions (Azam et al., 2019). The ideal pH range for this precipitation typically lies between 8.5 and 10 (Jaffer, 2002; Çelen, 2007). However, competing ions like potassium and calcium can hinder struvite formation; potassium can create potassium struvite (KNH_4PO_4), while calcium competes to form calcium phosphate, often leading to a reduced yield of struvite.

Calcium phosphate also precipitates under conditions similar to those for struvite, occurring when calcium ions react with phosphate at neutral to alkaline pH levels. Competing precipitation of calcium with carbonate present naturally in wastewaters leads to decreased CaP

yield due to calcite formation. It can be effectively controlled by the removal of the alkalinity, as shown recently (Kannan, 2023). The resulting precipitates are typically either amorphous or poorly crystalline, serving as effective slow-release phosphorus fertilizers, especially in acidic soils where calcium phosphates exhibit increased solubility (Vogel et al., 2017).

Both struvite and calcium phosphate have been tested as slow-release fertilizers, with studies showing varied results based on soil conditions and plant species. For instance, experiments have indicated that struvite recovered from swine wastewater enhanced lettuce yields compared to traditional fertilizers (Lee, 2017). Additionally, calcium phosphate products have shown effectiveness in acidic soils, where phosphorus availability improves due to lesser precipitation with calcium and magnesium (Saliu & Oladoja, 2021). Recent developments in nanotechnology have broadened their applications, primarily through engineered nano calcium phosphate (nano-CaP) fertilizers designed to improve nutrient delivery and plant resilience to climate stressors. For example, avocado seedlings treated with nano-CaP under simulated drought and temperature stress displayed a 10–22.5% reduction in physiological decline, showcasing their potential utility in tropical environments (Ramirez-Gil, 2023).

Soil pH significantly affects nutrient availability. The ideal pH range for optimal plant uptake is between 6.5 and 7.5. In acidic conditions, phosphorus tends to bind with iron and aluminum, while in alkaline environments, it typically precipitates with calcium and magnesium, reducing its accessibility. These interactions highlight the necessity of aligning fertilizer choice with soil conditions.

1.3.2 Ion Exchange for ammonia adsorption

Ion exchange and adsorption-based processes have garnered attention as effective methods for ammonia recovery from wastewater. Among these methods are zeolites, which are

widely utilized due to their high cation exchange capacity (CEC), strong selectivity for ammonium (NH_4^+), low cost, and ability to function under varying load conditions (Koon & Kaufman, 1975; Huang et al., 2010). Natural zeolites are microporous aluminosilicate minerals featuring a tetrahedral framework of silicon (Si^{4+}), aluminum (Al^{3+}), and oxygen atoms. This framework contains exchangeable cations, such as sodium (Na^+), potassium (K^+), calcium (Ca^{2+}), and magnesium (Mg^{2+}), which ammonium ions can substitute in solution (Williams, 2015). This ion exchange process forms the basis for ammonia adsorption onto zeolites.

The ammonia adsorption capacity of natural zeolites varies significantly depending on their mineral composition, particle size, surface area, and pre-treatment processes. Reported values range from 2.7 to 30.6 mg NH_4^+/g (Wang & Peng, 2010), with performance also affected by the presence of competing cations in the wastewater matrix. Pre-treatment with sodium chloride (NaCl) to create homoionic Na^+-form zeolites is a standard method for enhancing ammonium exchange capacity. This treatment increases the exchangeable sodium content, which improves selectivity and ion exchange kinetics (Booker et al., 1996; Weatherley & Miladinovic, 2004).

A significant advantage of clinoptilolite is its capacity for regeneration, allowing for repeated use in ammonium removal processes. Studies have demonstrated that clinoptilolite maintains substantial ammonium removal efficiency after multiple regeneration cycles. For instance, research indicates that biologically regenerated clinoptilolite retains approximately 95.45% of its adsorption capacity (Martins, 2016). The longevity of clinoptilolite's effectiveness through regeneration varies across studies. In some cases, clinoptilolite has been effectively regenerated and reused for up to 12 cycles without notable degradation in ammonium removal capacity (Wang, 2010). It is important to note that the efficiency of regeneration is likely

dependent on factors such as the regeneration method employed, the presence of competing ions, and the specific wastewater matrix

Regeneration of ammonium-saturated zeolites often involves alkaline brine solutions (e.g., NaOH or NaCl), which can restore ion exchange capacity but introduce secondary waste management issues (Zhang et al., 2017). As an alternative to regeneration, nutrient-loaded zeolites can be directly applied as slow-release fertilizers, thereby closing the nutrient loop (Renata Jarosz, Justyna Szerement, Krzysztof Gondek, Monika Mierzwa-Hersztek, 2022). Several studies have examined the fertilizer potential of ammonium-saturated zeolites. For instance, (Kocatürk-Schumacher et al. 2019) demonstrated that clinoptilolite enriched with ammonium from anaerobic digestate improved nitrogen uptake and biomass production in ryegrass compared to controls. Similarly, sustained nitrogen release and enhanced crop yield following the application of NH_4^+-loaded zeolites, suggesting their value in controlled-release formulations (Li, 2013). Zeolite-amended soils improve nutrient retention and enhance cation exchange buffering, improving soil fertility over time (Bansiwal, 2006). Despite promising results, broader adoption of ion exchange–based nutrient recovery products faces several barriers. Concerns around product consistency, nutrient composition, purity, and comparison with conventional fertilizers must be addressed to improve market viability (Kogler, 2021).

1.3 Research Objectives

The primary objective of this research project is to develop and optimize nutrient recovery systems for ammonia and phosphorus from AnMBR-treated swine wastewater. The first phase focuses on evaluating ammonia recovery using clinoptilolite adsorption. This involves modeling and demonstrating an ammonia absorption curve for a single clinoptilolite-packed column and comparing the results to models developed in previous studies, such as those by

Arvind. Building on this model, a three-column system operated in series will be designed to maximize adsorption capacity while ensuring that the effluent ammonia concentration remains below 25 mg/L NH_3-N. Additionally, a desorption curve will be created using 0.5M NaCl brine water to understand better the kinetics of ammonium release, which is essential for the regeneration and reuse of the adsorption media.

The second objective of the research aims to optimize sequential phosphorus recovery through the precipitation of struvite and calcium phosphate. This will involve evaluating different recovery sequences and magnesium-to-phosphorus ratios to maximize phosphorus removal, targeting over 80% total phosphorus recovery. The characteristics of the recovered solids were assessed to evaluate their potential as fertilizer products, considering both nutrient content and agronomic value. To further enhance the scalability and feasibility of real-world applications, the study investigated the kinetics of precipitation reactions. Also, it evaluated alternative alkalinity removal strategies such as pH adjustment and duration of aeration. Ultimately, the feasibility of scaling up the optimized sequential recovery process (from 2-L to 60-L volume AnMBR permeate) was assessed to evaluate its practical application in real-world wastewater treatment systems.

Chapter 2 - Adsorption and Desorption of Ammonia from Swine Wastewater Permeate: Modeling of Naturally Occurring Clinoptilolite Packed Bed Columns

2.1 Introduction

As global food demands rise, so too has the use of N on crops. This rise has resulted in a 380% increase in inorganic nitrogen fertilizers in the US alone from 1961 to 2022 and a 1100% increase worldwide during the same period (FOASTAT, 2024). Globally, only 50% of the N fertilizer applied to crops is absorbed, with the rest being lost to the environment from runoff affecting surface water (Eickhout, 2006).

Clinoptilolite has emerged as a versatile natural zeolite with significant potential in wastewater treatment, particularly for resource recovery applications. Its high cation exchange capacity, chemical stability, and selectivity for ammonium ions make it an attractive candidate for ammonia recovery from agricultural waste streams (Lin., 2015). However, while its application has been demonstrated in drinking water and municipal wastewater systems, there remains a critical gap in the literature regarding its use in swine wastewater, characterized by elevated ammonia concentrations, competing ions, and highly variable composition.

This variability highlights the need for a robust and predictive model to support long-term column operation. Ion exchange behavior can be very sensitive to influent conditions, and without a dynamic operational framework, column performance may degrade prematurely. Previous studies have noted challenges related to clinoptilolite's channel heterogeneity and its effects on saturation rates and breakthrough behavior (Ferronato et al., 2015). Furthermore, while modified or pretreated clinoptilolite has demonstrated improved removal efficiencies

(Mitrogiannis et al., 2017; Vasquez et al., 2022), few investigations have examined how these materials function over time in real, complex swine wastewater environments.

In this chapter, we evaluate the performance of clinoptilolite-packed columns in treating AnMBR-treated swine permeate. This includes developing a predictive model for breakthrough behavior, validating the model with experimental data, and assessing regeneration through brine desorption. The findings provide insight into clinoptilolite's operational limits and recovery potential, ultimately contributing to the advancement of nutrient recovery strategies for high-strength agricultural wastewaters.

2.2 Materials and Methods

2.2.1 Clinoptilolite characteristics

The natural zeolite used in this study was clinoptilolite, which was selected for its high cation exchange capacity (CEC) and known affinity for ammonium ions. The clinoptilolite was obtained from Zeobest and used in this study to remove ammonia (purchased from Northern Filter Media Inc., Iowa, USA). The vendor provided the chemical composition of the clinoptilolite media, which is shown in Table B.1. The total cation exchange capacity for ammonium-N was reported to be between 1.2 and 1.8 meq/g clinoptilolite, according to the manufacturer's specifications. Before use, the clinoptilolite was sieved and rinsed thoroughly with 18 ohm deionized (DI) water to remove excess fines, loosely bound particles, and exchangeable sodium ions. This rinsing step was especially critical to minimize the initial sodium release into the effluent, which was collected for use in a parallel study involving hydroponic cultivation and reduced ammonia permeate treatment through constructed wetlands. Elevated sodium levels in the column effluent could have negatively impacted plant performance.

2.2.2 AnMBR-treated swine permeate characteristics.

The influent used in all adsorption studies was treated swine permeate from K-State's anaerobic membrane bioreactor system. Table B.2 summarizes the average composition of the AnMBR permeate used in this study. Ammonium concentrations typically ranged from 600–1200 mg NH_4^+-N/L.

2.2.3 Glass adsorption columns

Glass columns were custom-fabricated at the Kansas State University Chemistry Glass Shop. Each column had an internal diameter of 2.5 cm, a height of 15 cm, and a total volume of 73.63 cm^2. The columns were packed with 250 g of air-dried, 1–3 mm sieved clinoptilolite. The zeolite was gently packed to ensure uniform bed porosity and prevent channeling. The column was operated in a bottom-up flow configuration to promote even distribution of influent and minimize air entrapment. The swine AnMBR permeate was fed to the base of the column using a Karnox KXP100 peristaltic pump, operated at a constant flow rate of 10 mL/min.

Effluent samples were collected from the column outlet at 1-hour time intervals. Ammonium concentrations in the effluent were measured hourly until the column was fully saturated, which was defined as the point where the concentration ratio (C/C_0) equaled 1. Here, C represents the ammonium concentration in the effluent and C_0 represents the influent ammonium concentration.

2.2.4 Kinetic Modeling of the Regeneration Curve

Following the adsorption phase described in Section 2.2.3, a column was subjected to a regeneration cycle to evaluate the desorption kinetics of ammonium from clinoptilolite using a saline solution. After a column fully saturated ($C/C_0 \approx 1.0$) during adsorption, the influent feed was switched from swine AnMBR permeate to a 0.5 M sodium chloride (NaCl) solution. The

brine was prepared in 10-liter batches using deionized water to ensure consistency. All other parameters remained consistent with the adsorption setup described in Section 2.2.3. The columns remained packed with the same 250 g of clinoptilolite, and the 0.5 M NaCl solution was fed in an upflow configuration using the same Karnox KXP100 peristaltic pump, operated at 10 mL/min. Effluent samples were collected hourly to monitor ammonium release until negligible concentrations of NH_4^+-N were observed in the effluent.

The ratio of desorbed ammonium concentration to the initial ammonium concentration in the influent (C/C_0) was plotted as a function of time to develop desorption curves. These curves were analyzed using the same kinetic modeling approaches applied in the adsorption study (Thomas model and Yoon-Nelson model), providing insight into ion exchange reversal's regeneration efficiency and kinetics under sodium-dominated conditions.

2.2.5 Continuous Run of Three Packed Columns in Series

The continuous-flow experiments were conducted using three packed-bed columns operated in series. This configuration was designed to extend breakthrough time and maximize ammonia removal, while producing a large volume of low-ammonia effluent suitable for downstream reuse studies. Each column was fabricated identically to those described in Section 2.2.3 and packed with 250 g of rinsed clinoptilolite. The columns were arranged in series, with the effluent from the first column feeding directly into the second, and the effluent from the second into the third. This arrangement allowed for sequential polishing of the AnMBR swine permeate as it passed through each stage. The system was operated continuously using the same Karnox KXP100 peristaltic pump set at a constant 10 mL/min flow rate. The columns were bottom-fed to maintain even flow distribution.

Operation continued until 40 liters of treated effluent were collected from the outlet of the third column, with the final effluent ammonia concentration consistently below 25 mg/L NH_4^+-N. This concentration threshold was selected based on reuse requirements for the hydroponic constructed wetland study and to evaluate best practices to maximize ammonia adsorption on the clinoptilolite. Effluent samples were collected at regular intervals throughout the run and analyzed for ammonia content.

Following initial trials, a predictive modeling approach was developed to track breakthrough behavior and optimize column performance. This allowed for strategic rearrangement of the columns between runs based on prior adsorption loading. Specifically, a pattern was followed in which the lag column—typically experiencing only partial saturation ($C/Co < 0.5$) due to its placement at the end of the series—was rotated to the lead position in subsequent runs. The remaining two columns were freshly regenerated with unused clinoptilolite to ensure continued performance. This approach enabled more efficient use of spent media while maintaining the final effluent ammonia concentration below the 25 mg/L NH_4^+-N target. Figure [X] indicates which column configurations involved reused clinoptilolite and reflects the column order for each continuous run.

2.2.6 Analytical Methods

All ammonia concentration measurements were performed using the salicylate method (Hach Method 10031) and analyzed on a Hach DR3900 spectrophotometer. The minimum detection limit for this method was 0.02 mg/L NH_4^+-N, with all readings taken in duplicate to ensure accuracy. Any samples with concentrations above the measurable range were diluted appropriately using deionized water. pH measurements were conducted using a calibrated Thermo Scientific™ Orion Star™ A211 pH meter, calibrated daily using standard buffer

solutions at pH 4, 7, and 10. Effluent samples were collected directly from the column outlet at designated intervals and either analyzed immediately or stored at 4°C for no more than 24 hours before analysis.

2.3 Results and Discussion

2.3.1 Kinetics of Ammonia Adsorption

Following the procedure described in 2.2.3, the performance of natural clinoptilolite for ammonium removal was evaluated using a continuous-flow fixed-bed column. Swine AnMBR permeate with an influent ammonia concentration of 1068 mg/L was passed through a column packed with 250 g of natural clinoptilolite at a 10 mL/min flow rate. The column was monitored over a 7-hour period, with effluent samples collected hourly to observe the onset and progression of breakthrough. The first detectable concentration of ammonia in the effluent occurred at the 3-hour mark, indicating the practical breakthrough point of the media. Up to this point, the column had treated a total volume of 1.8 liters of permeate, corresponding to a total ammonia removal of approximately 1.92 g. When normalized to the mass of the clinoptilolite used (0.25 kg), the calculated ammonia loading at breakthrough was 7.68 mg/g.

The empirical adsorption capacity observed in this study aligns well with values previously reported by the research group for clinoptilolite. Batch equilibrium tests conducted both as part of this study and in prior work by the research group yielded a maximum ammonium adsorption capacity of approximately 13.5 mg/g. The breakthrough observed at 7.68 mg/g in the continuous-flow column corresponds to approximately 57% of the total capacity. These results are consistent with those reported by Kannan (2022), who reported a breakthrough capacity of 5.55 mg/g under similar column testing conditions but with a lower influent concentration (400 mg/L) and slower flow rate (1 mL/min). The slight increase in breakthrough loading observed in

this study may be attributed to the higher influent ammonia concentration, which increases the driving force for ion exchange and results in faster saturation of exchange sites.

2.3.2 Breakthrough Curve Modeling

The kinetic behavior of ammonia adsorption onto clinoptilolite was evaluated using breakthrough data from a single-column experiment with swine AnMBR permeate. The breakthrough curve (Figure 2.1) followed a typical S-shaped profile, with negligible effluent ammonia in the first few hours and a sharp concentration rise near saturation. Effluent samples were collected every hour, and ammonium concentrations were analyzed using salicylate. The data was normalized by dividing effluent concentrations (Ct) by the influent concentration (Co = 1069 mg/L) to obtain a dimensionless breakthrough ratio Ct/Co

The Thomas model was applied to model the adsorption kinetics. This model assumes Langmuir-type sorption kinetics and negligible axial dispersion and is widely used to predict breakthrough behavior in fixed-bed column systems. Both linear and nonlinear approaches were considered to fit the model to the experimental data.

$$\ln\left(\frac{C_o}{C_t} - 1\right) = \frac{k_{Th} q_o M}{Q} - k_{Th} C_o t$$

where k_{Th} is the Thomas rate constant (mL/mg/min), q_o is the maximum adsorption capacity (mg/g), M is the mass of the adsorbent (250 g), Q is the flow rate (10 mL/min), and t is time in minutes.

Initial attempts to fit this model using a full range of sampling points yielded an extremely high and unrealistic adsorption capacity (e.g., q_0>13,000 mg/g), far beyond the expected range for natural clinoptilolite (typically 10–15 mg/g). This poor fit could be attributed to two primary causes:

1. Nonlinearity of the early curve segment, especially between t=0 and 180 minutes, where the ammonia breakthrough was negligible, and the slope of the breakthrough curve was essentially flat.

2. Sparse intermediate data, with only a single data point between the onset of breakthrough and near-saturation. This resulted in a steep curve rise and introduced significant error into the regression slope and interception.

To improve the reliability of the linear model, a subset of data points was selected from the intermediate breakthrough region, where $0.1 < C_t/C_0 < 0.95$. This approach follows the recommendation by Runping Han, who noted that fitting the model within this range yields a more representative estimation of the kinetic parameters (Han, 2007). Using this refined data set (collected at 240, 300, and 360 minutes), the linear regression yielded a slope of −0.0226 and an intercept of 13.41. From these values, the Thomas rate constant was calculated as K_{th} – 2.12*10^-15 and the adsorption capacity as q_o = 54.58 mg/g. This capacity is still significantly higher than expected, although more reasonable than the earlier results. It suggests that the linearized model may still be prone to overestimation due to the limited number of data points in the most informative region of the breakthrough curve. The relatively sharp rise between 240 and 360 minutes may amplify fitting errors in linear regression models due to the logarithmic transformation.

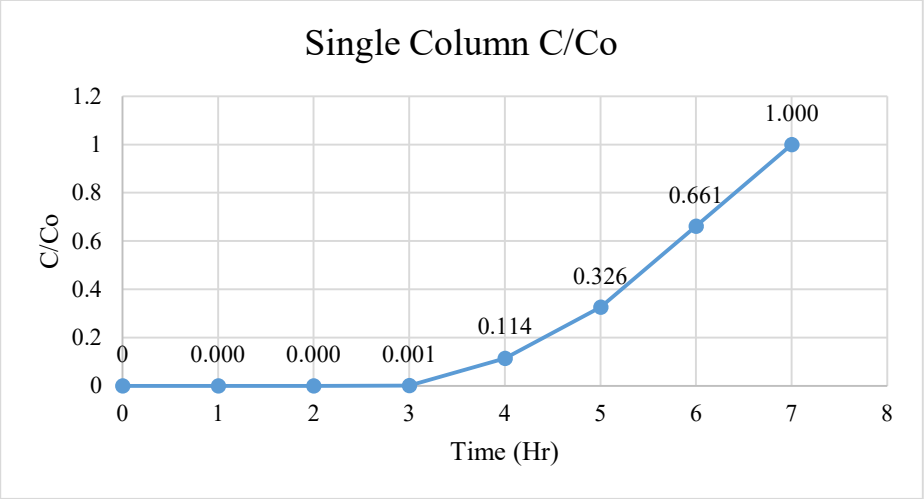

Figure 2.1: Observed C/Co values for a single clinoptilolite-packed column treating ammonia-rich swine permeate over time. The column exhibited a typical sigmoidal breakthrough curve, reaching full saturation (C/Co = 1) after approximately 7 hours, with an initial breakthrough point observed near 4 hours.

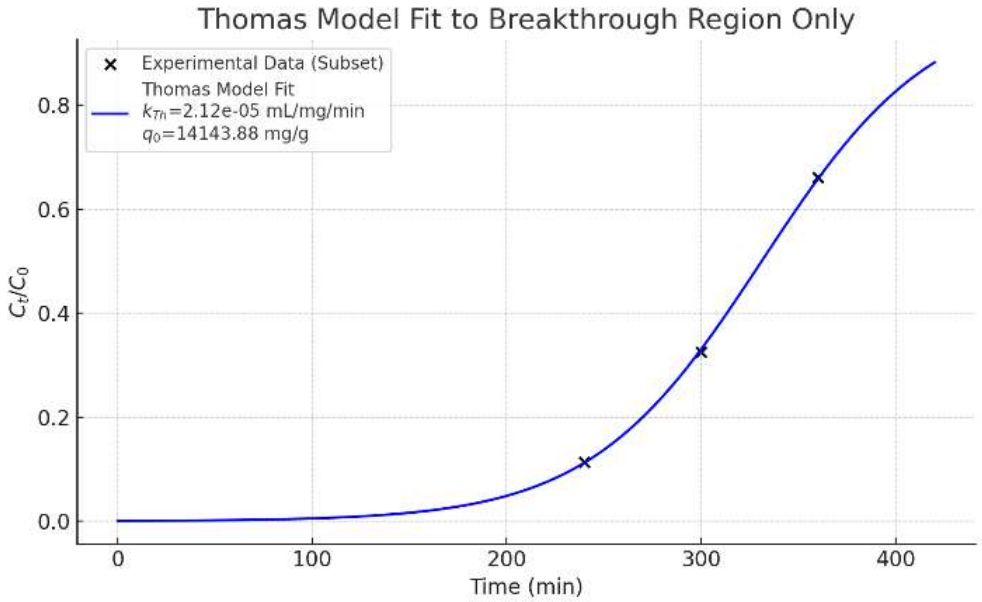

Figure 2.2The Thomas model curve is fitted to the breakthrough portion of empirical data from the single-column trial.

Despite the limitations of the Thomas model in this study, the empirical breakthrough behavior closely aligned with trends reported in previous research, including that of Kannan (2022). Notably, clinoptilolite typically reaches breakthrough after adsorbing approximately 50%

of its maximum capacity, prompting the development of a predictive spreadsheet model to simulate breakthrough behavior in a system of three clinoptilolite-packed columns operated in series. The model incorporates empirical uptake estimates and assumes a breakthrough threshold of ~50% for each column, enabling iterative calculation of effluent ammonia concentrations over time. This modeling approach effectively reproduces the overall shape and trend of the effluent concentration curve observed in multi-column experiments. It provides a practical framework for designing and operating ammonia recovery units coupled with a stringent effluent ammonia-N goal, in wastewater treatment systems.

2.3.2: Continuous Run of Three Packed Columns in Series

After validating the breakthrough kinetics and developing a predictive model for ammonia loading, the next phase of this study focused on testing the system's performance under extended, real-world conditions. The objective was to operate three clinoptilolite-packed columns in series for a prolonged duration, achieving high overall ammonium adsorption while maintaining effluent concentrations below 25 mg/L NH_4^+-N. This threshold was selected in coordination with the Kansas State Constructed Wetlands Team, which uses the final effluent as a nutrient source for cattail-based hydroponic research. "Maximizing" ammonium adsorption in this context refers to intentionally operating the lead columns beyond their initial breakthrough points—where C/Co approached or exceeded 1.0—while ensuring that the final, lag column remained sufficiently unsaturated to polish the effluent and meet the ammonia target. The predictive model guided this process, allowing informed decisions on run time and column replacement or rotation. This approach reflects the operational constraints of decentralized treatment systems, where balancing media usage and treatment performance is critical to cost-effective nutrient recovery.

However, prior to the development of the breakthrough model, a 64-hour continuous trial was conducted using three clinoptilolite-packed columns operated in series. The objective was to maximize ammonium removal while maintaining effluent concentrations below 25 mg/L. However, without a predictive model to guide column rotation and timing, column performance varied significantly over the course of the run. As shown in **Figure 2.3**, influent concentrations remained between 507 and 633 mg/L. However, effluent ammonia values ranged widely, from as low as 2.66 mg/L to as high as 110 mg/L, indicating inconsistent media utilization and early breakthrough in some instances.

The mass of ammonium removed per kilogram of clinoptilolite also varied considerably across sampling intervals, ranging from 5.97 to 11.45 g/kg. This inconsistency highlights the limitations of relying solely on timed operation or qualitative indicators, particularly under variable loading conditions. These results motivated the development of a predictive breakthrough model based on empirical data to improve operational consistency and efficiency.

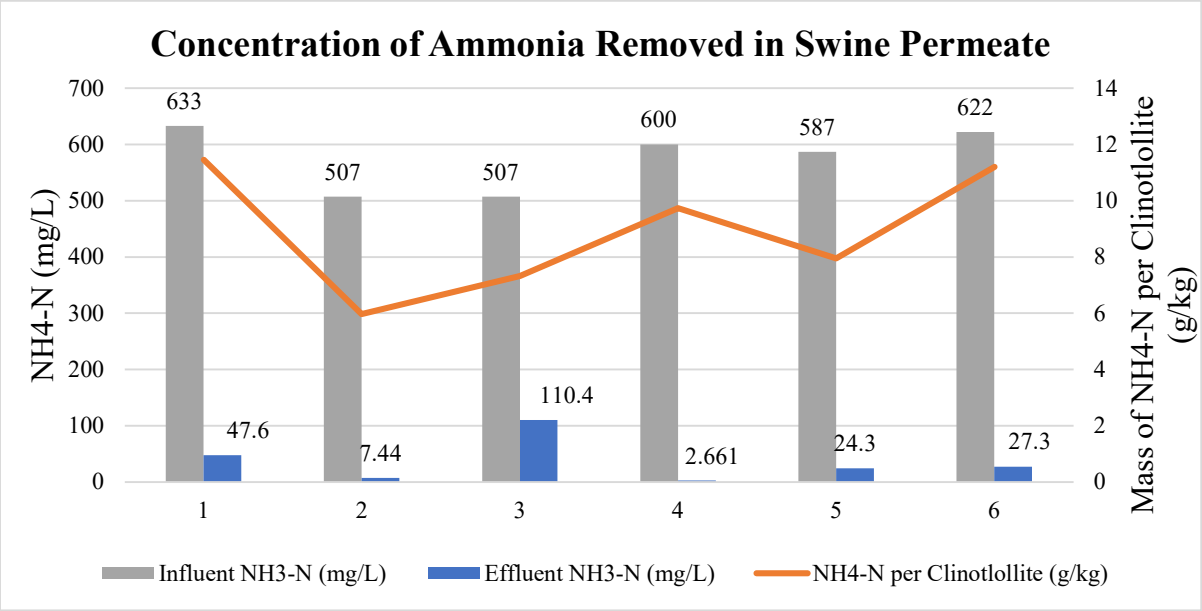

Figure 2.3: Ammonia effluent concentrations from the initial adsorption trials using three clinoptilolite-packed columns without breakthrough curve modeling. Early breakthrough

was observed with concentrations exceeding 100 mg/L with lower adsorption capacity <10 mg NH4-N/ clinoptilolite.

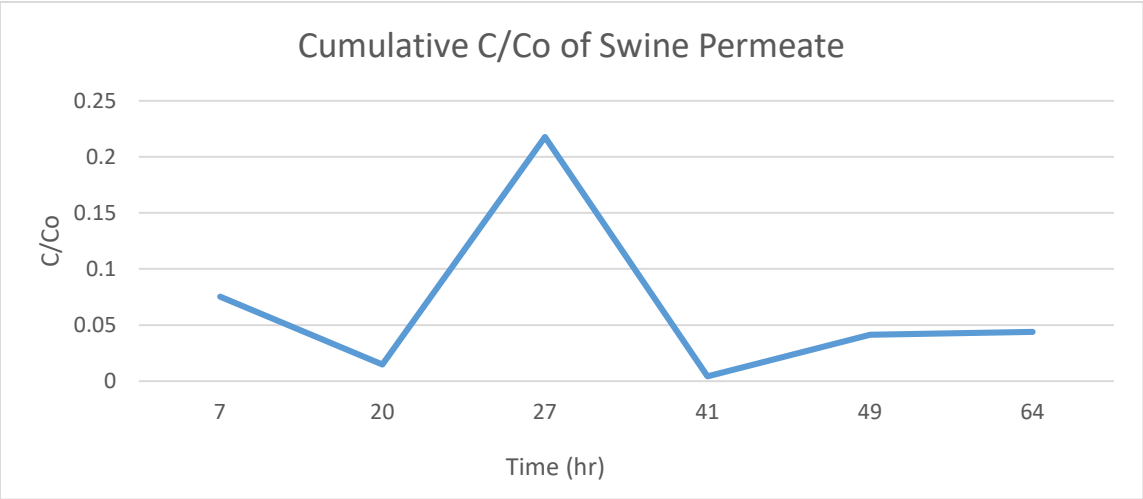

Figure 2.4: Breakthrough profile of the column system showing a C/Co ratio exceeding 0.2 during peak loading events. These elevated values resulted from a lack of flow control and predictive modeling, leading to inefficient adsorption and early column exhaustion during the initial trial.

A second trial was conducted using the predictive breakthrough model to guide operations to improve performance and maximize media utilization. Columns were sequentially connected as lead and lag columns, and rotated based on an estimated 50% breakthrough capacity, and effluent samples were monitored closely to confirm model predictions. As shown in Figure 2.5 influent ammonia concentrations remained high throughout the trial (ranging from 463 to 818 mg/L). Nevertheless, effluent values were maintained well below the 25 mg/L threshold in nearly all cases, except a single brief exceedance (33.5 mg/L) during the third sampling point.

Ammonia adsorption per kilogram of clinoptilolite showed greater variability than expected in this run, ranging from 3.6 to 16.26 g/kg. However, this trial achieved the highest observed ammonium loadings across all experiments, with peak values of 14.09 g/kg and 16.26

g/kg recorded toward the end of the run. These results suggest that, while variability remained due to factors such as fluctuating influent concentrations and real-world operation, the model effectively extended the usable lifespan of each column. By predicting when columns were nearing breakthrough and enabling proactive rotation, the system successfully pushed the media closer to its full adsorption potential without significantly exceeding effluent thresholds.

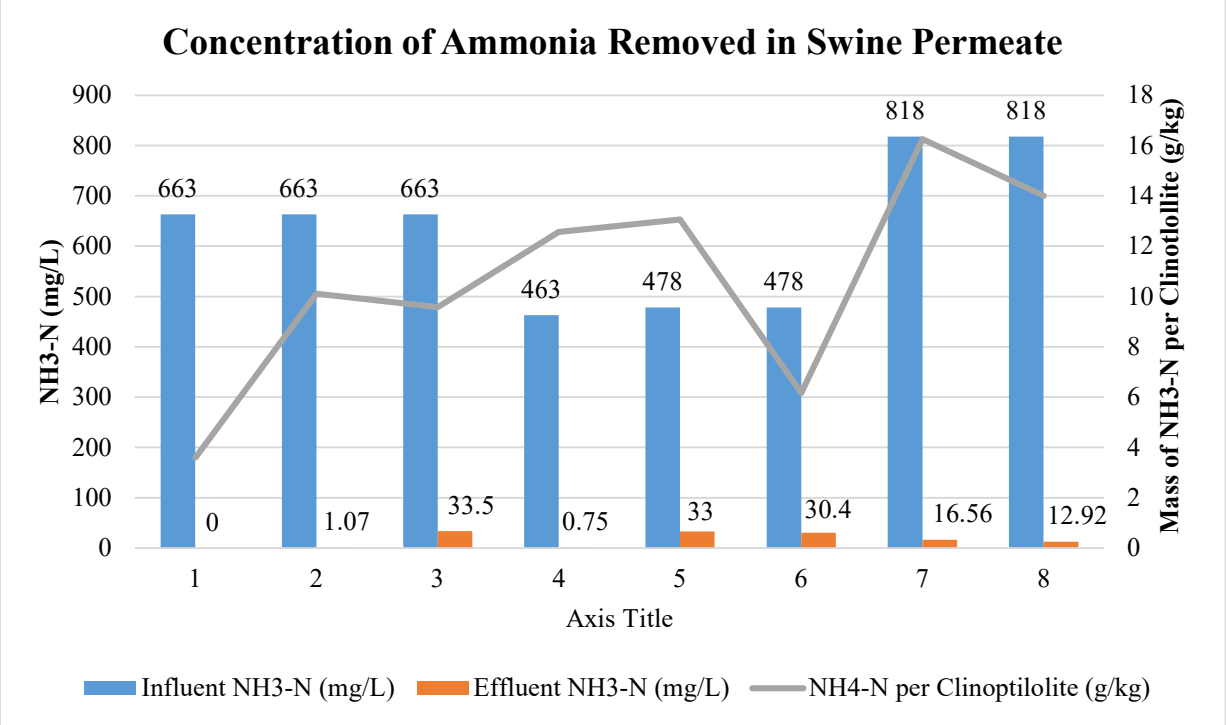

Figure 2.5: Influent and effluent ammonia concentrations across eight loading cycles using breakthrough modeling for optimized flow control. Effluent NH_3-N remained below 35 mg/L throughout the trial, resulting in significantly higher adsorption (up to ~16.56 g NH_4^+-N/kg clinoptilolite), indicating improved column utilization and delayed breakthrough.

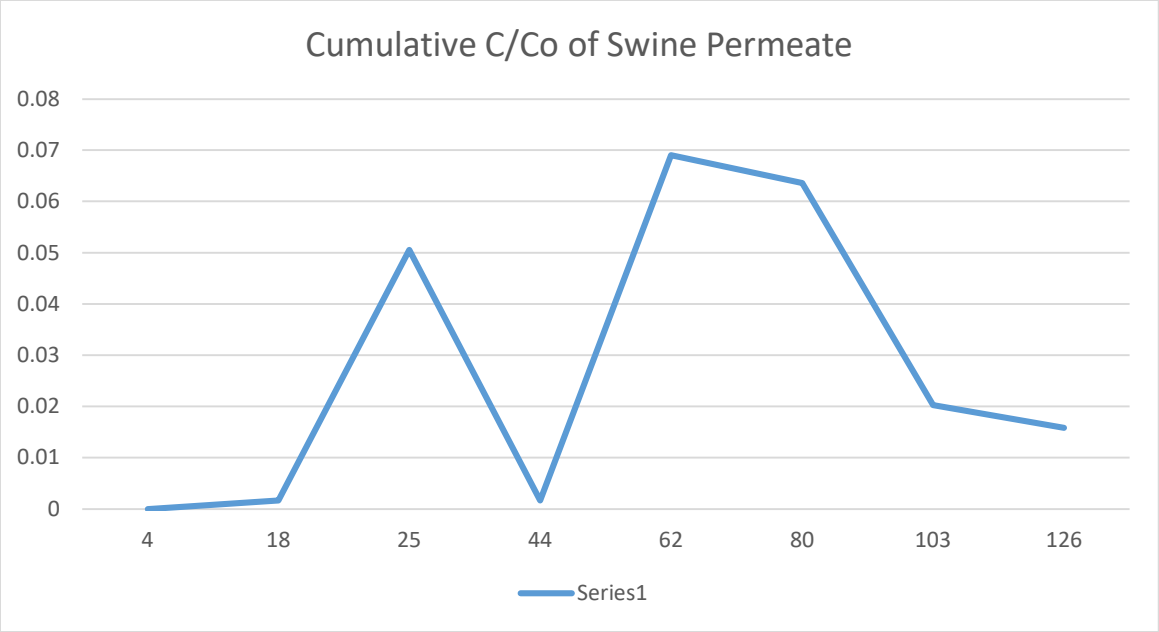

Figure 2.6: C/Co values over time remained consistently low, never exceeding 0.1. This demonstrates effective breakthrough control and tighter ammonia removal performance, reflecting the improved predictive dosing and flow strategy introduced during this trial.

Cumulative C/C_0 values were tracked across both extended trials to monitor the relative breakthrough and effluent ammonia concentrations over time. As shown in Figure 4, the first trial—operated without predictive modeling—exhibited erratic C/C_0 behavior, with values ranging from 0.02 to over 0.21. These fluctuations reflect inconsistent column rotation and early breakthrough events, resulting in elevated ammonia concentrations in the effluent during multiple intervals. In contrast, the second trial, shown in Figure 6, was conducted under more stringent operational control using the predictive model. C/C_0 values remained below 0.08 throughout the 126-hour duration, with most samples below 0.05, demonstrating improved effluent quality and more effective breakthrough management.

Despite maintaining lower C/C_0 values, the second trial achieved higher total ammonia adsorption per kilogram of clinoptilolite, confirming that more efficient media utilization can occur even under tighter effluent constraints. These results reinforce the value of proactive

column monitoring and model-guided operation in extending media lifespan and improving treatment consistency.

2.3.3 Kinetics of Ammonia Desorption

Following the adsorption trials, desorption experiments were conducted to evaluate the regeneration potential of clinoptilolite and to characterize the ammonium release profile under brine treatment. Columns that were fully saturated, reaching a C/Co value equaling 1, were regenerated utilizing a 0.5 M NaCl solution administered at the identical flow rate (10 mL/min) and in the same upflow configuration as articulated in Section 2.2.4. Effluent samples were collected hourly, and ammonia concentrations were analyzed to construct the desorption curve depicted in Figure 2.7.

The desorption breakthrough curve illustrates a pronounced initial release of ammonia, with effluent concentrations surpassing 1400 mg/L in the initial hour of brine application. This swift release indicates the high concentration gradient and the efficacy of sodium ions in displacing ammonium from the clinoptilolite exchange sites. Over the subsequent hours, ammonia concentrations rapidly declined, falling below 400 mg/L after 3 hours and nearing <50 mg/L by hour 6. Minor quantities of ammonia persisted in the effluent until hour 9, although concentrations remained below 30 mg/L. This curve signifies that the majority of ammonium can be extracted from clinoptilolite within the initial 3–5 hours of regeneration. The tailing behavior beyond this juncture is characteristic of slower exchange from internal diffusion zones or less accessible sites. These findings demonstrate that clinoptilolite can be effectively regenerated employing low-strength brine, and a single pass of brine over 8–9 hours suffice to recover most of the adsorbed ammonia. The regenerated ammonium-rich solution may also hold potential for reuse or recovery in downstream nutrient reuse systems.

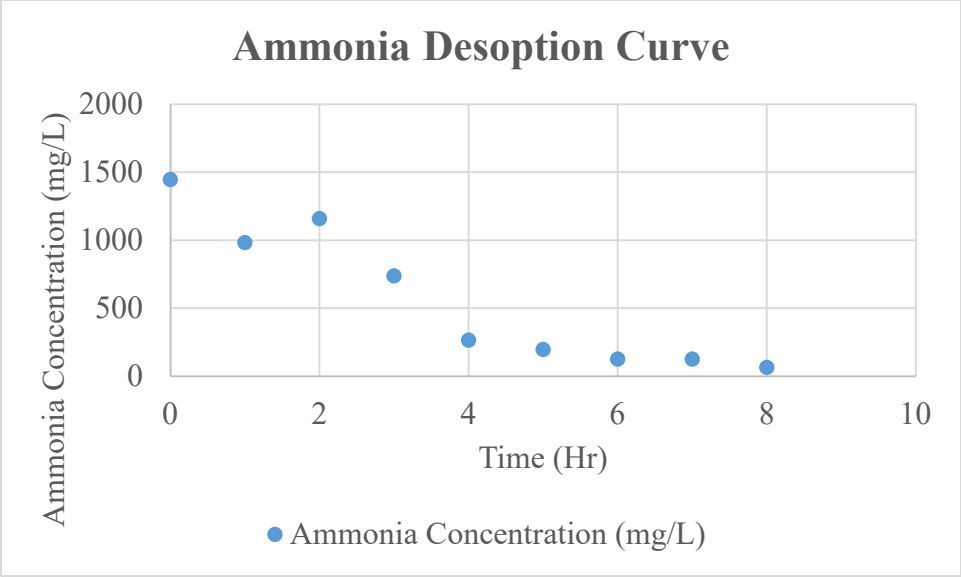

Figure 2.7: Ammonia desorption curve from a saturated clinoptilolite-packed column regenerated using 0.5 M NaCl solution.

2.4 Conclusion

This research demonstrates the efficacy and operational potential of natural clinoptilolite for ammonia removal from swine wastewater permeate, particularly when integrated with predictive modeling strategies. Initial single-column trials confirmed the characteristic breakthrough behavior of clinoptilolite, with empirical adsorption capacities reaching up to 7.68 mg/g before saturation. While traditional Thomas models showed limitations due to data sparsity and curve nonlinearity, the results nonetheless supported the development of a more practical, spreadsheet-based breakthrough model.

The application of this model in a three-column system significantly improved performance. Compared to earlier trials that lacked flow control, the model-guided operation consistently achieved lower effluent concentrations (<25 mg/L NH_4^+-N) while pushing clinoptilolite toward its full adsorption potential (up to 16.26 g/kg). These results highlight proactive column management's importance in enhancing media utilization and maintaining effluent quality under variable loading conditions.

Finally, desorption studies confirmed that clinoptilolite can be effectively regenerated using a 0.5 M NaCl solution, with most ammonium being recovered within the first five hours of treatment. The regeneration curve revealed rapid initial exchange followed by diminishing returns—a behavior consistent with ion diffusion limitations. The regenerated solution, rich in ammonia, presents an opportunity for downstream nutrient recovery. Collectively, these findings support the implementation of clinoptilolite-based adsorption columns as a viable ammonia polishing step in decentralized treatment systems, offering both high removal efficiency and recovery potential when paired with simple predictive tools.

Chapter 3 - Sequential Phosphorus Recovery of Struvite and Calcium Phosphate

3.1 Introduction

Struvite ($NH_4MgPO_4 \cdot 6H_2O$) is a valuable phosphate mineral found in both natural and engineered systems, particularly in wastewater treatment plants (WWTPs) where magnesium (Mg^{2+}), ammonium (NH_4^+), and phosphate (PO_4^{3-}) are present in favorable ratios (Doyle & Parsons, 2002). While uncontrolled struvite precipitation can cause scaling issues in pipelines and reactors, which increases maintenance costs and reduces hydraulic capacity (Achilleos et al., 2022; Petzet & Cornel, 2012), controlled struvite recovery provides significant economic and environmental benefits. Recovered struvite is an effective slow-release fertilizer, making it a key target for recovery P in municipal wastewater systems (Melia et al., 2017). Full-scale struvite recovery operations, such as those at the Boise, Idaho WWTP, showcase its feasibility and commercial viability.

Phosphorus recovery through mineral precipitation offers a sustainable pathway to reclaim valuable nutrients from high-strength wastewaters such as anaerobic membrane bioreactor (AnMBR) permeate. While struvite precipitation has been widely demonstrated due to its predictable formation under controlled pH and magnesium dosing, it is not the only phosphate mineral of interest. Calcium phosphate (CaP) precipitation has also gained attention as a viable recovery route in swine treated permeate (Kannan., 2023).

However, effective CaP recovery presents several challenges. First, high alkalinity in the influent can interfere with CaP precipitation, requiring substantial acid dosing (e.g., HCl) to strip carbonate and adjust pH. Although aeration has been shown to reduce this acid demand by off-gassing CO_2, the alkalinity removal step remains a key chemical constraint. Once the competing

alkalinity is sufficiently removed, CaO dosing can be optimized, enabling the exploration of Ca:P molar ratios between 0.5:1 and 2:1 to improve removal efficiency and product selectivity. Moreover, product quality is influenced by pH and carbonate conditions, with better specificity toward soluble forms of CaP such as octacalcium phosphate (OCP) when alkalinity is reduced.

Considering these constraints, sequential phosphorus recovery—combining CaP and struvite precipitation in a single treatment train—offers a promising route to maximize overall phosphorus recovery while minimizing chemical use. Nevertheless, studies exploring this sequence remain limited. A key optimization focus is the order of chemical dosing: reversing the conventional sequence to test CaO followed by $MgCl_2$ could mitigate calcium's known inhibitory effects on struvite formation while preserving CaP precipitation performance. Preliminary data and literature suggest magnesium has little inhibitory effect on CaP formation, making this reversed approach particularly attractive. This chapter explores these configurations and evaluates which recovery sequence—and under what dosing conditions—provides the most efficient and selective P removal from AnMBR-treated swine permeate. This study presents a novel approach: reversing the previously explored sequence of chemical addition to recover calcium phosphate first, followed by struvite. While existing literature prioritizes struvite formation by adding $MgCl_2$ before Ca-based precipitants, we investigate whether initial CaO dosing can improve P removal by precipitating CaP, leaving residual P for subsequent struvite recovery. This strategy is particularly promising for waste streams like anaerobic membrane bioreactor (AnMBR) permeate, where P speciation may favor sequential extraction.

The following sections detail experiments evaluating the reversed sequential recovery ($CaO \rightarrow MgCl_2$) from swine wastewater permeate, comparing it to traditional struvite-first approaches. By validating this unconventional order, the work advances the potential for

flexible, high-efficiency nutrient recovery, in which multiple marketable phosphorus products can be extracted from a single waste stream. Results demonstrate the feasibility of this method and its implications for scalable phosphorus recovery systems.

3.2 Materials and Methods

3.2.1 Sample Collection and Pre-treatment

An AnMBR-treated swine permeate was collected the morning of testing from a lab-scale AnMBR at Kansas State University, which treats real swine lagoon wastewater. This system treated actual swine lagoon wastewater under steady-state conditions, achieving >80% COD and >95% BOD removal. Permeate samples were collected on the morning of experimental runs to ensure freshness. Upon collecting the permeate, it underwent characterization analysis to establish baseline parameters critical for recovery experiments. Total phosphorus (TP) and reactive phosphorus (RP) were quantified using HACH TNT 844 and TNT 845 test kits (0.5–5 mg/L-P and 2–20 mg/L-P ranges, respectively), with measurements performed on a HACH DR 3900 spectrophotometer. pH was monitored using a calibrated Fisherbrand™ accumet™ AB150 benchtop meter. These parameters are summarized later in Table 5.X (to be inserted during final editing).

To mitigate carbonate interference with precipitation reactions, the permeate underwent acidification. Using 4 M hydrochloric acid (HCl), the pH was systematically lowered to ~4.5 while mixing on a stir plate (100 RPM). HCl was selected over sulfuric acid to avoid the formation of ammonium sulfate, which would represent an unintended ammonia drop and complicate subsequent struvite recovery. The acidified permeate was then left stirring continuously for 24 hours at room temperature (22±2°C) to facilitate CO2 removal. Post-

treatment alkalinity measurements confirmed >95% reduction in carbonate species, decreasing from initial values of ~3000 mg/L as CaCO3 to <100 mg/L.

3.2.2 Sequential Recovery of Struvite Followed by Calcium Phosphate

3.2.2.1 Experimental Procedure

The sequential recovery process began with struvite precipitation in carbonate-free permeate. Magnesium chloride ($MgCl_2$) was added to 1.5 L of pretreated permeate at four molar ratios (Mg/P = 1:1, 1.5:1, 2:1, and 4:1), calculated based on the initial phosphorus concentration. The solution pH was immediately adjusted to 8.5 ± 0.2 using 5 M NaOH, with the added volume recorded to assess chemical demand. To optimize crystal growth, the mixture underwent rapid mixing at 100 RPM for 2 minutes using a jar test apparatus (Phipps & Bird PB-900), followed by gentle mixing at 30 RPM for the remaining 24 hours. This two-stage mixing protocol promoted nucleation while minimizing shear-induced crystal breakage. The supernatant was carefully decanted to be reused in the next stage while the solid precipitate was collected. The solids were then transferred to an Eppendorf 5920 R centrifuge operated at 10,000 RPM for 20 minutes.

The filtered supernatant from struvite precipitation was subjected to calcium phosphate recovery by adding calcium oxide (CaO) at a fixed molar ratio of Ca:P = 4:1, determined from the residual phosphorus concentration measured post-struvite removal. The pH was then modified to 8.5 ± 0.2. To ensure consistent hydrodynamic conditions, the solution was mixed identically to the struvite stage (100 RPM → 30 RPM). The solids were then transferred to an Eppendorf 5920 R centrifuge operated at 10,000 RPM for 20 minutes.

Both struvite and calcium phosphate solids were air-dried at room temperature in a desiccator using W.A. Hammond Drierite as the desiccant. To assess reproducibility, duplicate runs were performed for each Mg/P ratio.

3.2.3 Sequential Recovery of Calcium Phosphate Followed by Struvite

3.2.3.1 Experimental Procedure

The sequential recovery followed the methodology described in Section 5.2.2.1, but with reversed precipitation order and modified parameters to account for calcium interference effects. Calcium phosphate precipitation was initiated first by adding CaO to pretreated permeate at Ca:P molar ratios of 0.5:1,1:1, 1.5:1, and 2:1. The 4:1 ratio was not used like the struvite-first sequence to minimize residual calcium in the permeate. The pH was maintained at 8.5±0.2 during 24 hours of mixing. (100 RPM for 2 min → 30 RPM for 23 hr 58 min) before centrifugation (10,000 RPM, 20 min). The calcium phosphate-depleted supernatant was then used for struvite recovery using $MgCl_2$ at Mg/P=1:1. All other procedures - including mixing regimes, centrifugation parameters, and drying methods - remained identical to those described in Section 3.2.2.1.

This reversed sequence was explicitly designed to test calcium's inhibitory role in struvite formation, as discussed in Section 3.2. The lower initial CaO doses and stringent pH control during the struvite stage represent critical deviations from the struvite-first protocol to enable meaningful comparison of the two approaches.

3.2.4 Analytical Methods

Reactive phosphorus concentrations were measured at each recovery stage (post-struvite and post-calcium phosphate precipitation) to determine removal efficiencies. Immediately after sampling, solutions were filtered through sterile 0.45 μm polyethersulfone (PES) syringe filters (Thermo Scientific™ Nalgene™, Cat. No. 194-0045) to exclude suspended precipitates that could artificially elevate readings. The filtered permeate samples were then analyzed using TNT 845 (2–20 mg/L-P) test kits, selected based on expected concentration ranges. Absorbance was

measured at 880 nm on a HACH DR 3900 spectrophotometer. Duplicate measurements were performed for each sample, with relative standard deviations (RSD) below 5%. pH measurements were conducted using a calibrated Thermo Scientific A211 pH meter, calibrated daily using standard buffer solutions at pH 4, 7, and 10. Samples were collected directly from the column beakers and either analyzed immediately or stored at 4°C for no more than 24 hours before analysis.

3.3 Results and Discussion

3.3.1 Struvite Precipitation Followed by CaP Recovery

The results of the first trial of MgCl2 followed by CaO chemical precipitation showed that P removal after Mg addition was >88% removal at all ratios, with the highest at 95% at the 4:1 Mg: P dose, as shown in Figure 3.1 below. The initial RP concentration was found to be 96.25 mg/L (PO43-P). Calcium addition at a Ca:P dose of 2:1 further removed 37.8% in the 4:1 Mg: P dosed permeate. The combined P removal for each Mg and Ca addition stage resulted in an overall removal efficiency of>93%, reaching 97%.

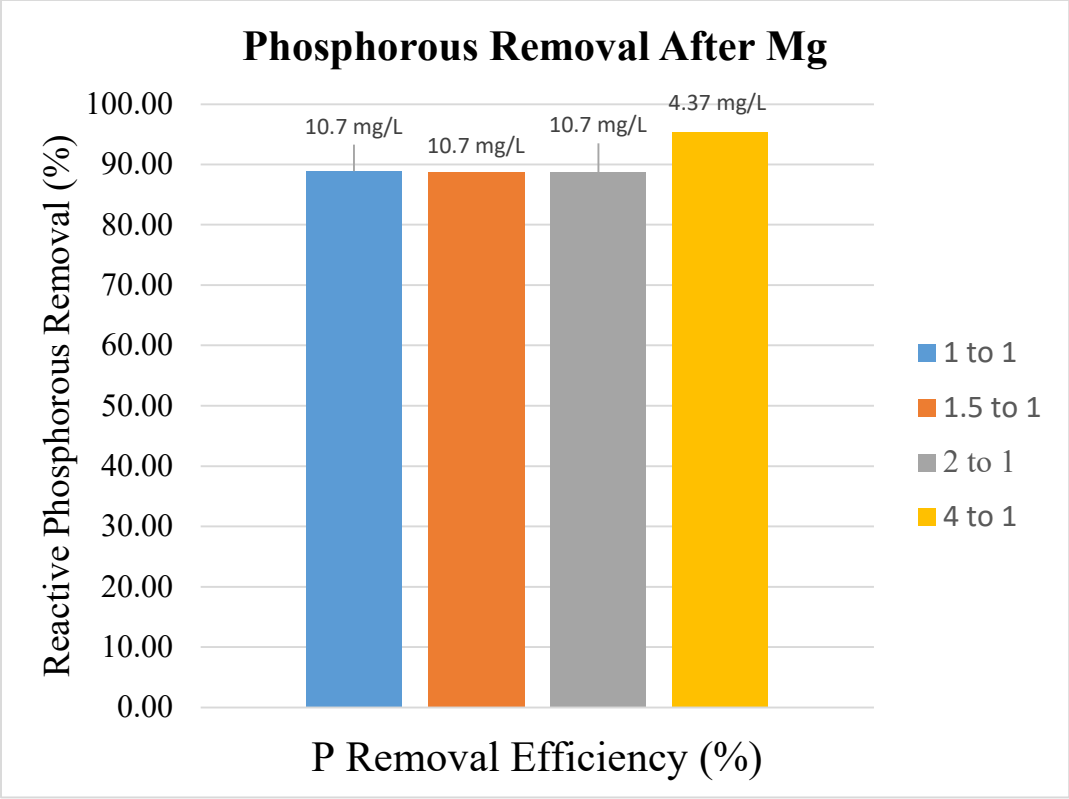

Figure 3.1: Phosphorus removal efficiencies following Mg:P dosing at ratios of 1:1, 1.5:1, 2:1, and 4:1, with initial PO_4^{3-}-P concentration of 96.25 mg/L. Results indicate similar P removal (~89%) at Mg/P ratios of 1:1 to 2:1, with a modest improvement to 95.5% at 4:1 Mg/P. Corresponding effluent P concentrations are labeled above each bar.

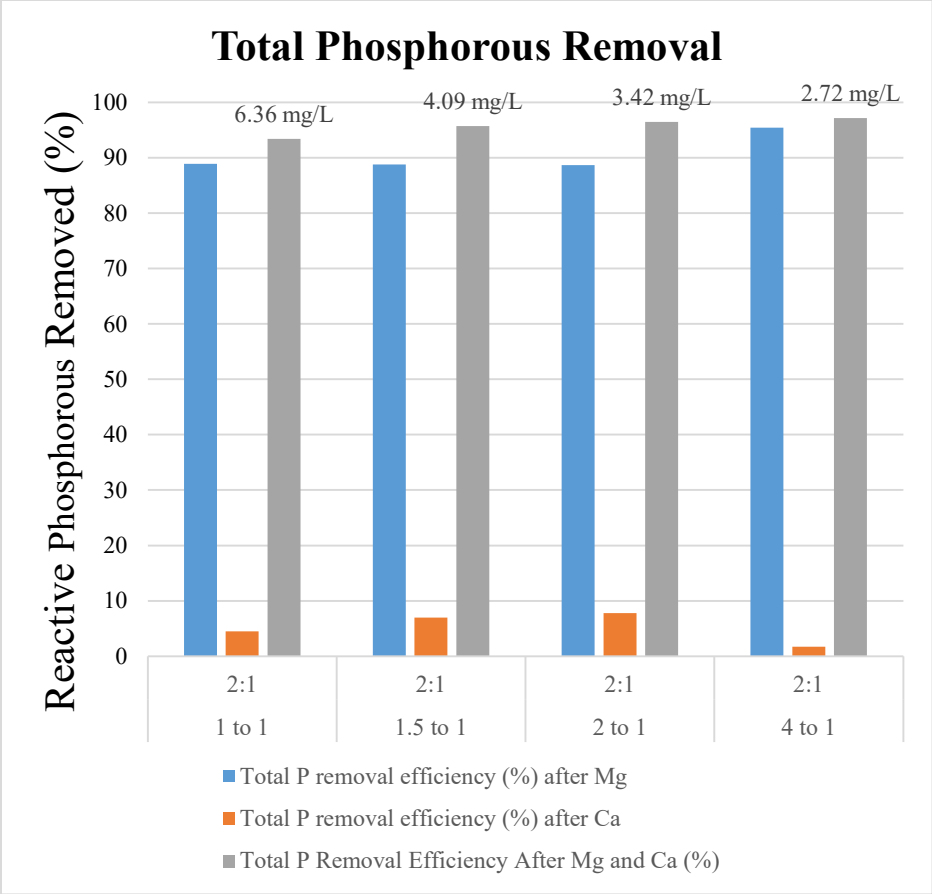

Figure 3.2: **Total phosphorus removal efficiencies from sequential Mg and Ca dosing at varying Mg/P molar ratios (1:1 to 4:1), followed by a fixed Ca/P dose of 2:1. Initial PO_4^{3-}-P concentration was 96.25 mg/L at pH 8.5. Blue bars represent phosphorus removal after Mg addition, orange bars show additional removal from Ca dosing, and green bars indicate total phosphorus removal. Maximum combined removal efficiency of 97.2% was observed at 4:1 Mg/P and 2:1 Ca/P, resulting in an effluent P concentration of 2.72 mg/L.**

The second trial saw similar results, with all Mg:P ratios achieving >90% P removal efficiencies. However, during this trial, it was observed that the sequential 2:1 Ca:P addition was less effective than the 4:1 ratio. The highest removal efficiency during this step was 11.1% in the 1:1 Mg: P permeate. There was, however, an additional 40% P removed in the 4:1 ratio.

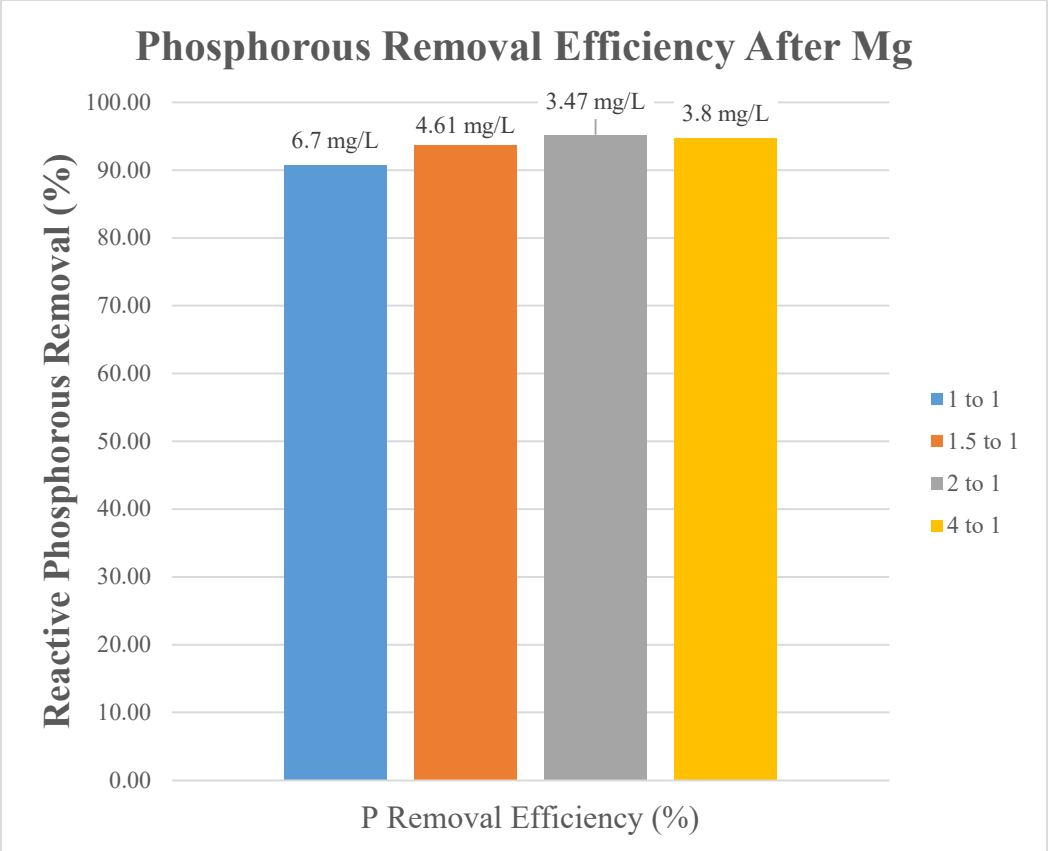

Figure 3.3: **Phosphorus removal efficiencies following $MgCl_2$ addition at varying Mg:P molar ratios (1:1 to 4:1) in Trial 2, with an initial PO_4^{3-}-P concentration of 72.8 mg/L. Effluent phosphorus concentrations ranged from 3.47 mg/L to 6.7 mg/L, with the highest removal (96.4%) achieved at a 2:1 Mg/P ratio.**

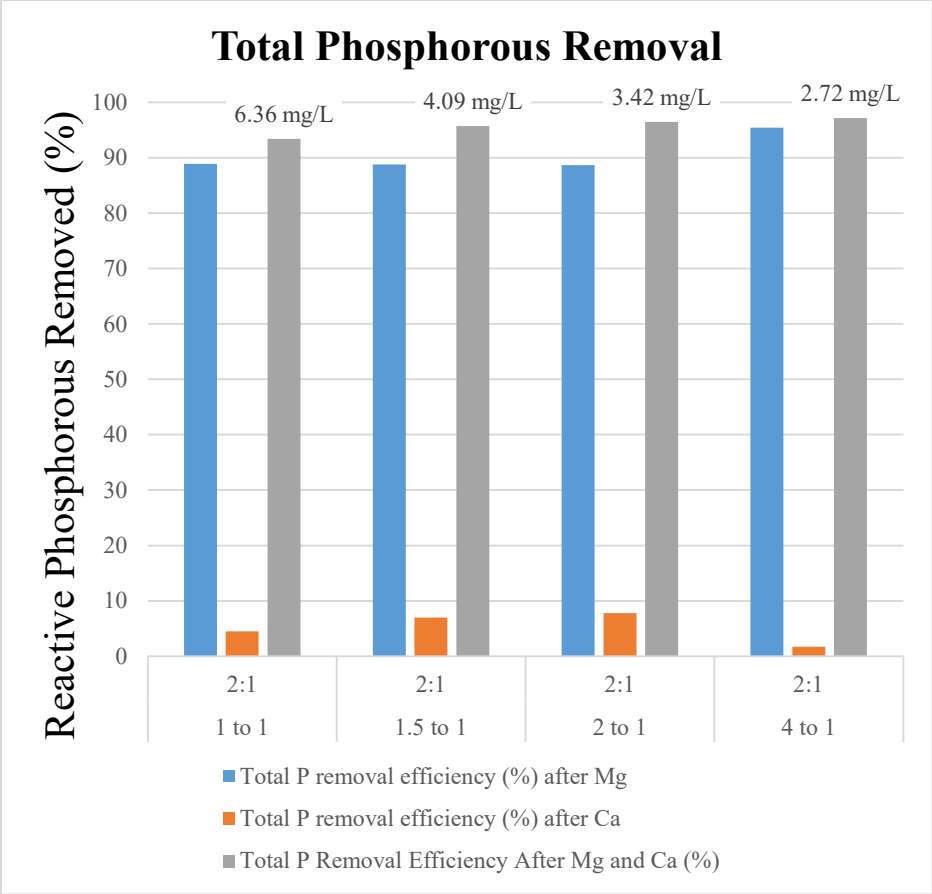

Figure 3.4: **Total phosphorus removal efficiencies following sequential $MgCl_2$ and CaO addition in Trial 2. Mg/P molar ratios ranged from 1:1 to 4:1, followed by a fixed Ca/P dose of 2:1. Initial PO_4^{3-}-P concentration was 72.8 mg/L. Combined Mg and Ca treatment achieved final effluent P concentrations between 2.72 mg/L and 6.36 mg/L, with the highest total P removal (97.2%) observed at the 4:1 Mg/P condition.**

Across both trials, the sequential dosing of Mg and Ca achieved total phosphorus removal efficiencies high enough to approach standard P discharge thresholds. At the highest Mg:P ratio of 4:1 followed by a 2:1 Ca:P dose, final effluent phosphorus concentrations reached as low as 2.72 mg/L. This corresponds to a 40–60% reduction of residual phosphorus following the initial Mg treatment step. These results suggest that the sequential chemical precipitation approach, particularly at elevated Mg doses, can reduce phosphorus concentrations to near the discharge

standards for treated effluent (typically 1–2.5 mg/L), highlighting the method's potential for application in decentralized or advanced treatment systems.

3.3.1.1 Ammonia Dynamics During Struvite Formation

In addition to phosphorus recovery, measurable ammonium removal occurred during the magnesium chloride dosing stage, supporting struvite formation ($MgNH_4PO_4 \cdot 6H_2O$). Initial ammonia concentrations across all Mg:P dosing conditions were consistent at 609 mg/L as NH_3-N. After struvite precipitation, ammonia concentrations decreased to between 406 and 481 mg/L, corresponding to removal efficiencies ranging from 21.02% to 33.99%. The highest ammonium removal (33.99%) was observed at the 1.5:1 Mg: P ratio, while the lowest (21.02%) occurred at the highest magnesium dose (4:1 Mg: P). These results suggest that while ammonia is effectively co-precipitated at lower Mg :P ratios, excess magnesium may hinder complete ammonia integration into the struvite crystal structure. Similar trends have been reported showing that adding more Mg^{2+} beyond the stoichiometric ratio (Mg:N:P = 1:1:1) does not significantly improve ammonia removal, as the reaction is limited by phosphate (Yetilmezsoy et al., 2017).

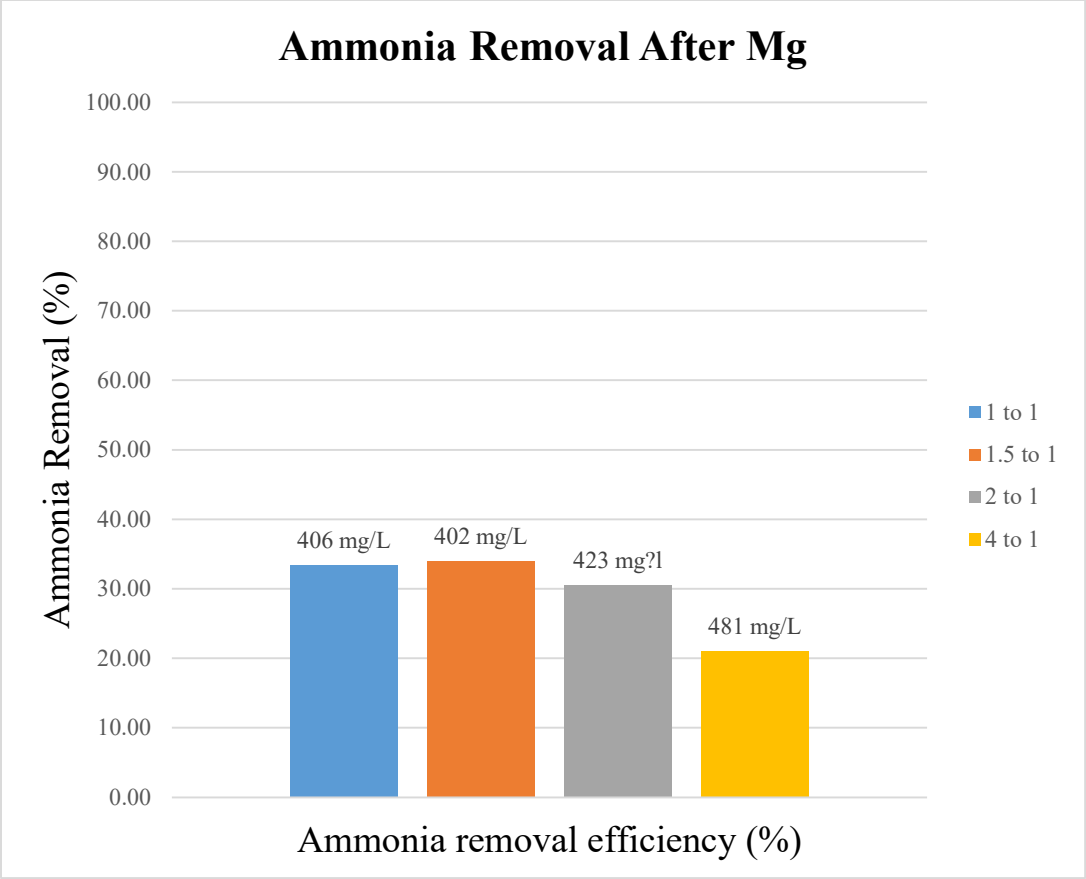

Figure 3.5: **Ammonia removal efficiencies following $MgCl_2$ addition at various Mg:P molar ratios (1:1 to 4:1) during trial 1, with an initial NH_3–N concentration of 609 mg/L. Removal efficiencies ranged from 21% to 35%, corresponding to effluent concentrations of 406–481 mg/L. Highest ammonia removal (35%) was observed at a 2:1 Mg/P ratio.3.3.1.2 XRD Characterization of recovered struvite**

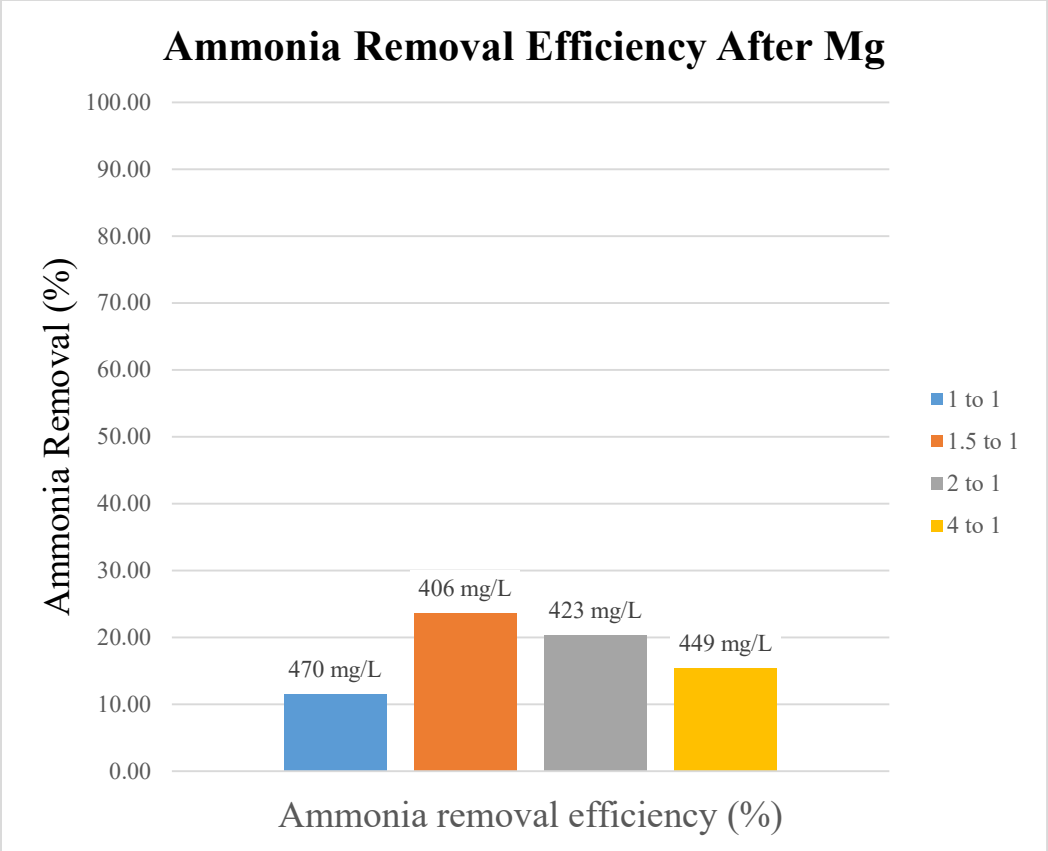

Figure 3.6: **Ammonia removal efficiencies following $MgCl_2$ dosing at varying Mg/P molar ratios (1:1 to 4:1) in Trial 2, with an initial NH_3–N concentration of 531 mg/L. Effluent concentrations ranged from 406 to 470 mg/L, corresponding to removal efficiencies between 11.5% and 23.6%. Maximum ammonia removal occurred at the 1.5:1 Mg/P ratio.**

During Trial 2, lower ammonia removal efficiencies were observed compared to Trial 1. However, these values more closely align with the theoretical 1:1:1 molar stoichiometry of struvite ($MgNH_4PO_4 \cdot 6H_2O$) formation, where the removal of phosphorus, magnesium, and ammonium should occur in approximately equal proportions. With only ~60 mg/L of phosphorus removed during the Mg dosing phase, similar levels of ammonium removal (~60 mg/L) are consistent with expected struvite precipitation behavior.

In contrast, the elevated ammonia removal observed in the previous trial may have resulted from unintentional losses due to volatilization or stripping during prior pH adjustments

or aeration steps. This highlights the importance of controlling experimental conditions, particularly pH and gas exchange, when evaluating ion recovery in chemically reactive systems. The results from Trial 2 provide a more representative benchmark for ammonium removal via struvite under controlled conditions.

3.3.1.2 XRD Characterization After Initial Struvite Step

The results of the XRD analysis, shown in Figure 3.6 the XRD pattern of the precipitate formed after Mg addition at Mg:P of 1:1. Phase analysis of the precipitates showed peak matching with struvite mineral, confirming struvite formation. The high intensities of the peaks seen around 15-16° angles compared to the pure struvite pattern were reported in a previous study and observed with increasing pH (7.8-9) and increasing Mg: P ratio (Liu et al., 2018).

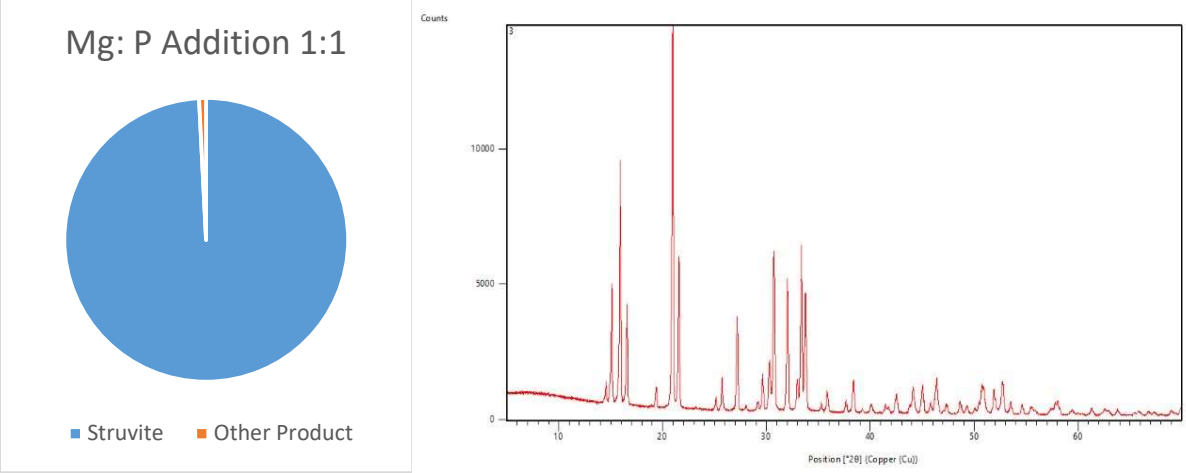

Figure 3.7: XRD pattern and phase composition of the precipitate formed following $MgCl_2$ addition at a 1:1 Mg:P molar ratio. The XRD spectrum shows characteristic peak alignment with struvite, confirming its formation as the dominant crystalline phase. The accompanying pie chart illustrates that struvite accounted for most of the crystalline composition.

3.3.2 Calcium Phosphate Precipitation Followed by Struvite

3.3.2.1 Phosphorus Removal Efficiency in Reversed Sequence

During the Ca:P trials, it was observed that increasing the Ca:P molar ratio led to a progressive improvement in phosphorus removal efficiency. At a Ca:P ratio of 0.5:1,

approximately 37–52% of reactive phosphorus was removed, which increased to 49–82% at a ratio of 1:1, 85–91% at 1.5:1, and peaked at 94–96% at 2:1. This suggests a strong dependence of phosphorus precipitation on calcium dosing, likely due to enhanced formation of calcium phosphate compounds at higher molar ratios.

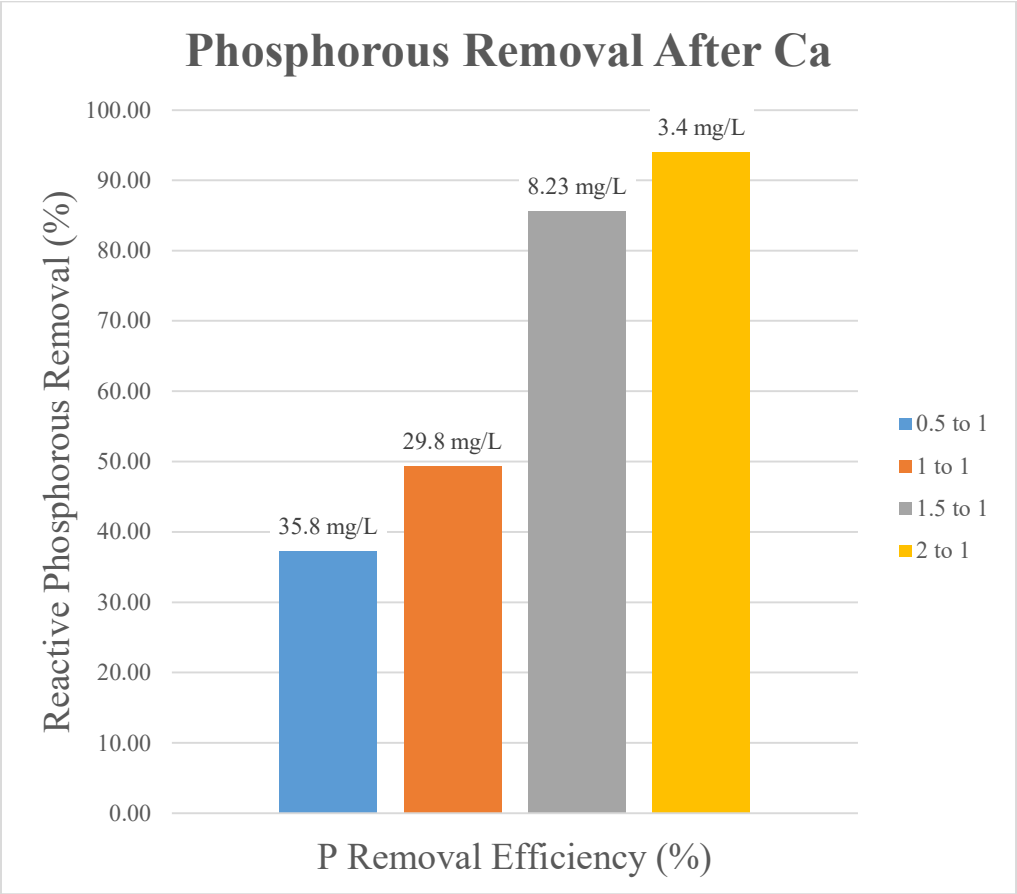

Figure 3.8: Phosphorus removal efficiencies following CaO addition at varying Ca: P molar ratios (0.5:1 to 2:1) in Trial 1, with an initial PO_4^{3-}-P concentration of 57 mg/L.

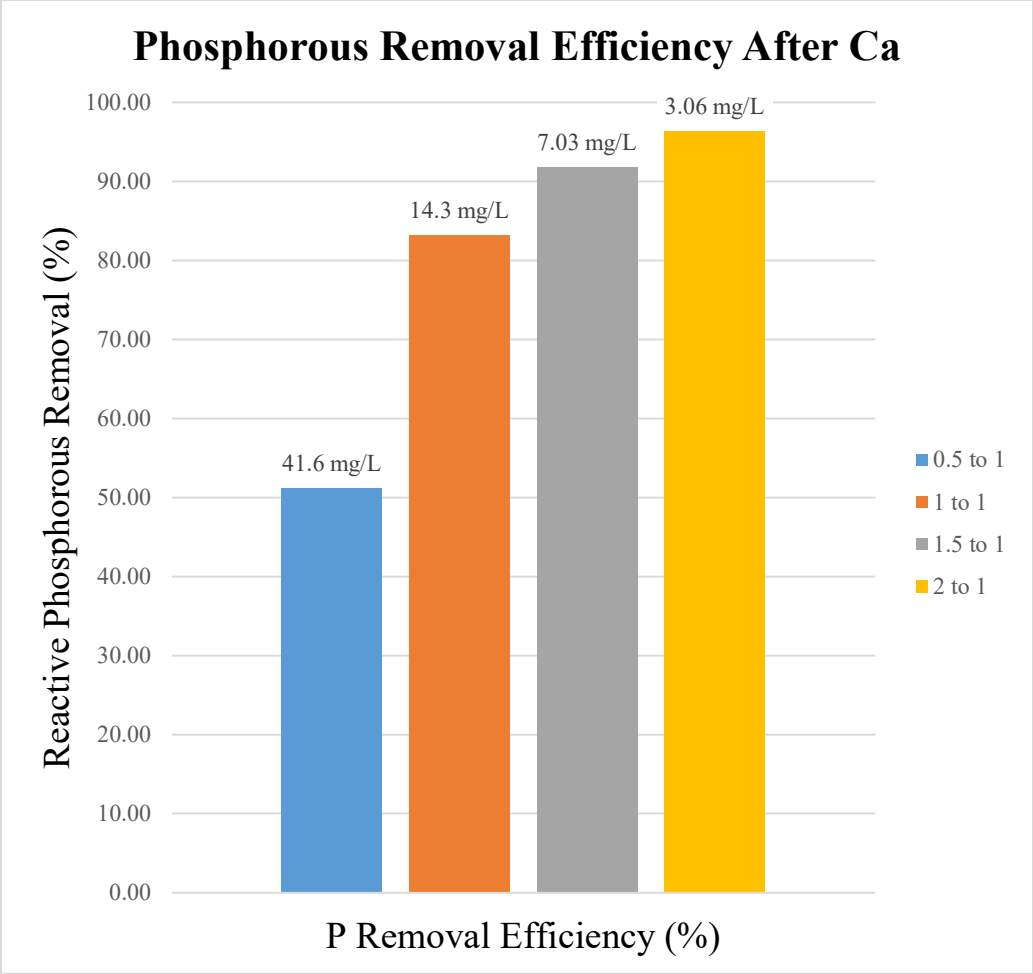

Figure 3.9: Phosphorus removal efficiencies following CaO addition at Ca:P molar ratios ranging from 0.5:1 to 2:1 in Trial 2, with an initial PO_4^{3-}-P concentration of 85.2 mg/L.

Despite variations in initial phosphorus concentrations between trials (~57 mg/L in Trial 1 and 85.2 mg/L in Trial 2), the removal percentages across Ca:P ratios remained consistent. This suggests that the molar ratio of Ca to P, rather than initial P concentration, is the dominant factor governing CaP precipitation dynamics under the tested conditions.

Adding Mg at a fixed 1:1 Mg:P ratio further enhanced overall phosphorus removal, although the benefit diminished at higher Ca:P ratios. For example, the 0.5:1 Ca:P trial achieved an additional 30–45% phosphorus removal after Mg addition, increasing the combined removal efficiency to 66–79%. At 1:1 Ca:P, the secondary Mg addition yielded a more modest 15–31%

additional removal. However, at Ca:P ratios of 1.5:1 and 2:1, only 0–20% additional removal was noted with Mg addition, as overall phosphorus removal efficiencies plateaued near 90–97%.

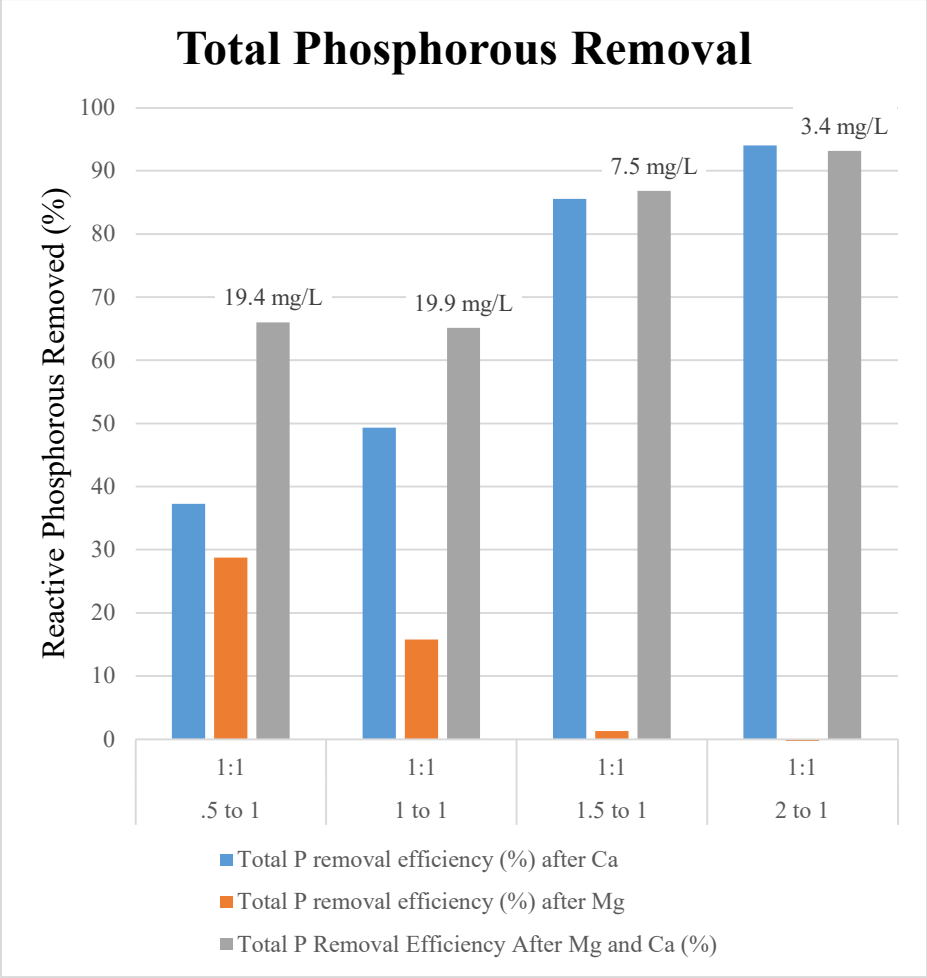

Figure 3.10: Total phosphorus removal achieved through sequential CaO and $MgCl_2$ addition in Trial 1. Ca:P molar ratios ranged from 0.5:1 to 2:1, followed by Mg:P dosing at 1:1. Initial PO_4^{3-}-P concentration was 57 mg/L. The combined removal efficiency peaked at 94.0% for the 2:1 Ca:P condition, reducing effluent P to 3.4 mg/L.

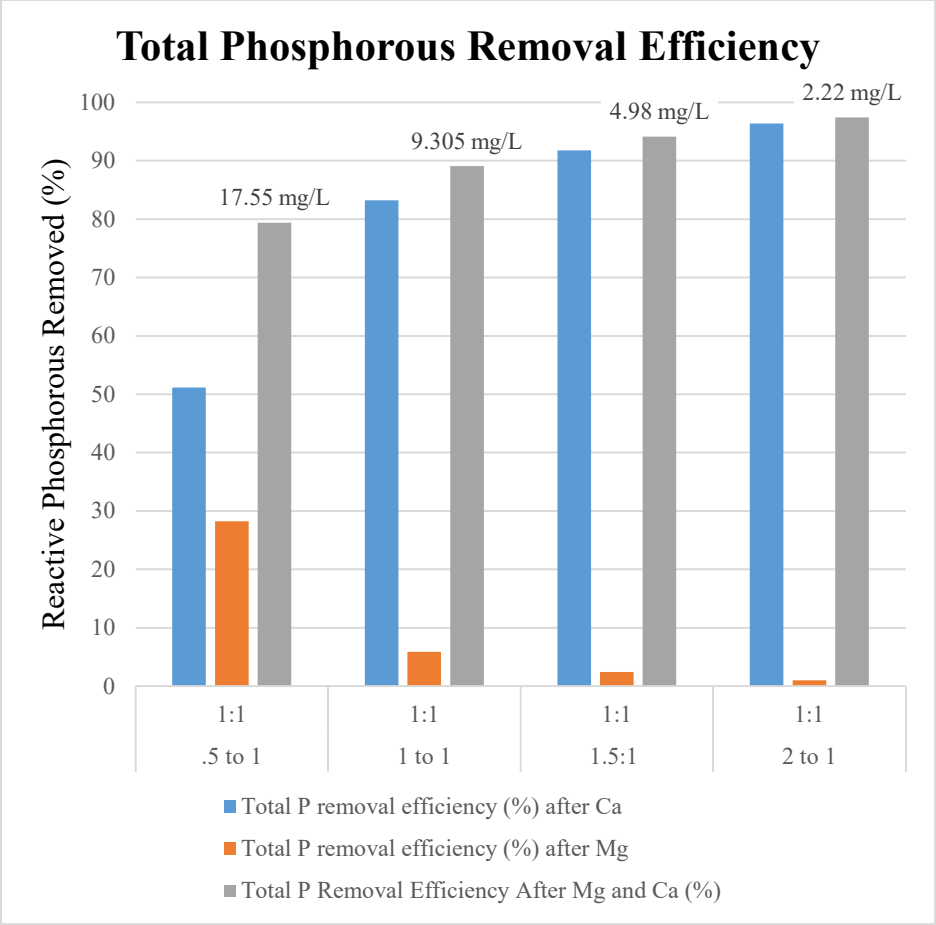

Figure 3.11: Phosphorus removal efficiencies following CaO addition at varying Ca:P molar ratios (0.5:1 to 2:1) in Trial 2, with an initial PO_4^{3-}-P concentration of 85.2 mg/L. The highest removal (96.4%) occurred at the 2:1 Ca:P ratio, reducing effluent P to 2.22 mg/L

This trend suggests that while initial calcium addition facilitates substantial phosphorus precipitation, the presence of residual calcium in the permeate may interfere with subsequent struvite formation by competing with magnesium ions for available phosphate. Consequently, the diminishing returns observed with Mg addition at higher Ca:P ratios highlight the importance of optimizing dosing sequences to maximize phosphorus recovery while minimizing reagent waste.

3.3.2.2 XRD Analysis of Sequential CaP–Struvite Formation

The order of chemical addition and the Ca:P molar ratio significantly influenced both the phase composition and solubility of the collected calcium phosphate (CaP) products. XRD phase analysis revealed significant variation in mineral composition across the three dosing conditions (0.5:1, 1:1, and 2:1 Ca:P), indicating a clear shift in precipitation pathways as calcium loading increased.

At the lowest Ca:P ratio of 0.5:1, the dominant phase was hydroxyapatite, with minor peaks corresponding to calcite ($CaCO_3$). The relatively broad peaks and the presence of calcite suggest partial precipitation of calcium as carbonate, likely due to residual alkalinity in the permeate even after acidification. While hydroxyapatite is a low-solubility, slow-release phosphorus product, its formation at this low Ca dose indicates that even modest calcium additions under controlled pH conditions can trigger selective phosphate recovery.

At 1:1 Ca:P, the product composition shifted toward a nearly pure octacalcium phosphate (OCP) phase. OCP is a metastable precursor to hydroxyapatite and exhibits greater solubility and bioavailability than HAP, making it suitable for applications requiring moderate-release phosphorus fertilizers. XRD peaks in this sample were slightly broader, suggesting a less crystalline or partially amorphous calcium phosphate product. This may improve plant-available phosphorus content depending on soil pH and conditions.

At the highest Ca:P ratio of 2:1, the recovered product consisted of a mixture of OCP, hydroxyapatite, and K_2HPO_4. The appearance of K_2HPO_4 is notable and suggests that residual potassium or buffering species in the permeate may participate in the precipitation reactions at elevated Ca levels. The presence of multiple crystalline phases and sharper diffraction peaks indicates a more heterogeneous and crystalline product compared to the lower-dose conditions.

These results highlight how the calcium dose not only governs phosphorus removal efficiency but also controls the type and structure of the recovered CaP. Lower Ca:P ratios favor single-phase or amorphous materials (such as OCP), whereas higher Ca dosing introduces multi-phase crystallization with potentially reduced solubility. From a fertilizer design perspective, this tunability offers flexibility to recover CaP products with different nutrient release rates—amorphous OCP for quicker release and crystalline HAP for long-term application.

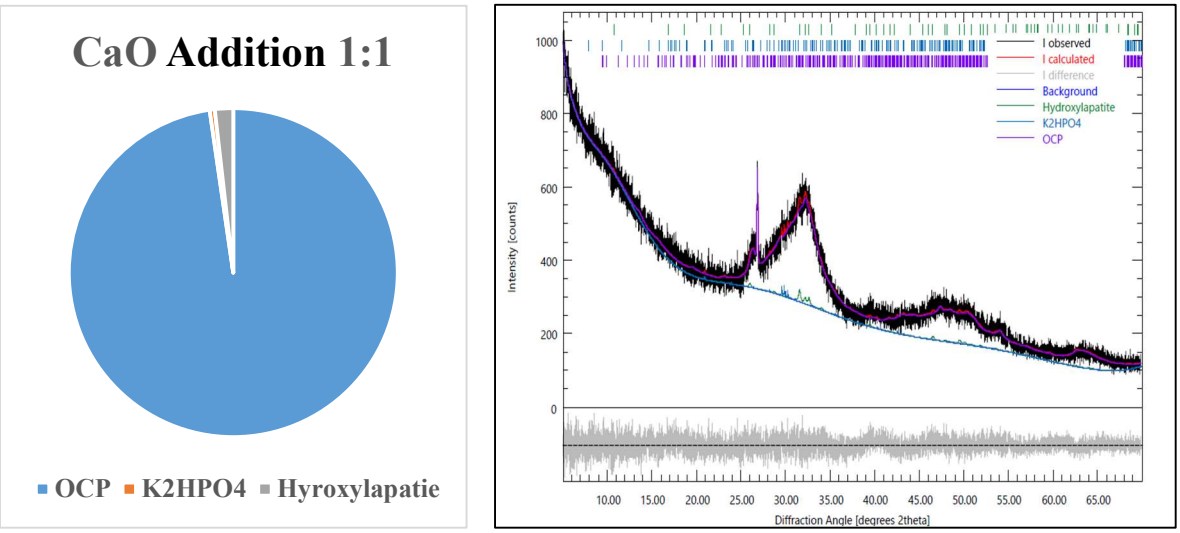

Figure 3.12: XRD analysis of the precipitate formed following CaO addition at a 1:1 Ca:P molar ratio in Trial 2. The dominant mineral phase is octacalcium phosphate (OCP), comprising 97.7% of the content. Minor phases included hydroxyapatite (1.8%) and K_2HPO_4 (0.5%). OCP is moderately stable and more soluble than hydroxyapatite, making it a plant-available form of phosphorus suitable for use as a slow-release fertilizer.

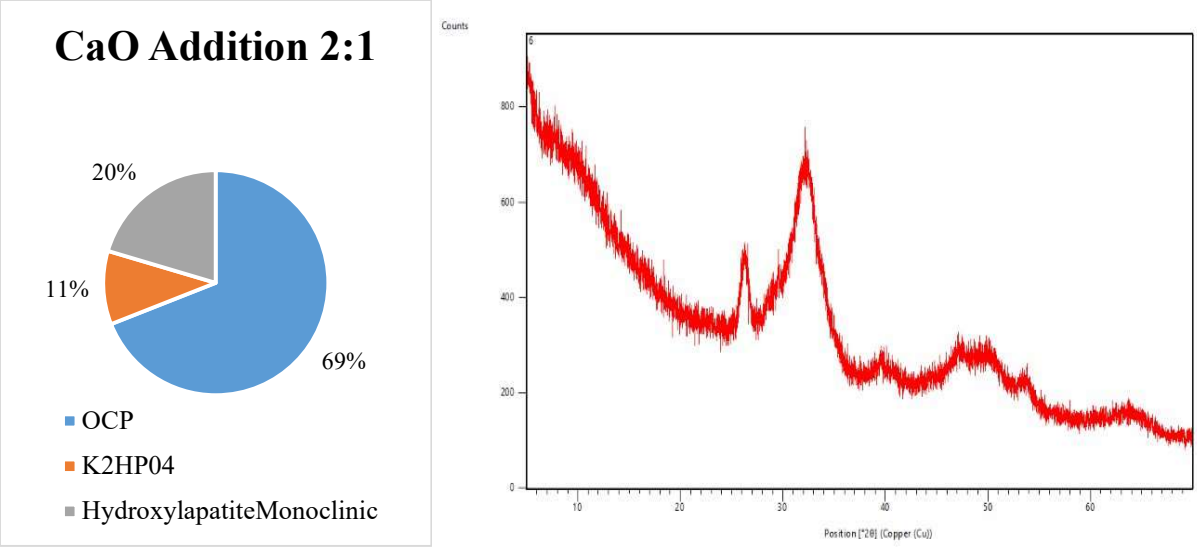

Figure 3.13: XRD pattern and phase composition of precipitates formed following CaO addition at a 2:1 Ca:P molar ratio in Trial 2. Quantitative phase analysis indicated octacalcium phosphate (OCP) as the dominant mineral phase (69%), with fractions of K_2HPO_4 (11%) and hydroxyapatite (20%). The presence of hydroxyapatite, a more crystalline and less soluble phase, suggests that higher Ca:P ratios promote formation of lower-solubility products, potentially impacting nutrient bioavailability when used as fertilizer.

3.4 Conclusions

The research presented in this chapter explored a novel, sequential phosphorus (P) recovery strategy that enables the targeted precipitation of two distinct P-based mineral products—struvite ($MgNH_4PO_4 \cdot 6H_2O$) and calcium phosphate (CaP)—from AnMBR-treated swine permeate. The findings from these experiments represent the first attempt to systematically compare and validate both struvite-first and CaP-first recovery pathways in a single integrated treatment train. This dual-product recovery system is particularly valuable in agricultural and circular nutrient economies, where struvite and CaP are slow-release fertilizers with complementary agronomic profiles.

The struvite-first process demonstrated consistently high phosphorus removal efficiencies, achieving >90% removal in all magnesium chloride ($MgCl_2$) dosing conditions and

up to 97% total P removal when followed by CaP precipitation via calcium oxide (CaO) addition. Increasing Mg:P ratios led to higher struvite yield, with the 4:1 molar ratio performing best in both recovery efficiency and downstream CaP performance. XRD analysis confirmed the formation of struvite, with some signal noise suggesting minor unidentified co-precipitates. Calcium addition to the struvite-treated permeate proved effective, although the efficiency of subsequent CaP recovery was more sensitive to remaining phosphorus concentrations and the Mg dose used upstream.

In contrast, the reversed order with CaP precipitation followed by struvite presented significant chemical and thermodynamic trade-offs. While CaO dosing alone was effective at Ca:P ratios ≥1.5:1 (achieving up to 94% P removal), residual calcium in the permeate posed a substantial inhibition to struvite formation in the second stage. As the Ca:P ratio increased, the ability of added Mg^{2+} to precipitate struvite dropped dramatically, with almost no struvite recovery observed following 2:1 Ca:P treatment. This supports previous findings that excess Ca^{2+} can interfere with struvite crystallization due to ionic competition and potential co-precipitation pathways (e.g., $CaCO_3$ or $CaHPO_4$ formation). Thus, in systems where struvite is the desired product, high Ca loads must be avoided or managed through selective precipitation or upstream removal.

Importantly, this research also showed that the two recovery sequences do not simply vary in efficiency, but also in how they handle residual ions and how each mineral phase influences the precipitation chemistry of the next. In the struvite-first approach, Mg removal and pH buffering facilitated favorable conditions for CaP recovery. Conversely, in the CaP-first approach, residual Ca created inhibitory conditions for struvite nucleation, requiring careful optimization of chemical dosing to mitigate these effects. From an operational standpoint, both

methods were shown to be reproducible and relatively simple to implement. They rely on common chemicals ($MgCl_2$, CaO) and minimal infrastructure beyond pH control, basic mixing, and solid-liquid separation. This makes the approach feasible for both centralized municipal treatment and decentralized livestock waste management systems, especially where nutrient reuse is prioritized.

The dual-product recovery strategy also presents flexibility in end-use applications. With its ammonium content and slow-release characteristics, Struvite is well suited for high-value horticultural and hydroponic systems. CaP, being more stable and calcium-rich, aligns with field-based agricultural systems and can be integrated into existing fertilizer regimes. By tailoring the precipitation sequence, operators can target specific recovery goals based on fertilizer needs, market value, or regulatory requirements for nutrient discharge.

Chapter 4 - Optimization of Sequential Recovery Processes

4.1 Introduction

The imperative for sustainable wastewater treatment extends beyond nutrient recovery; it also means minimizing energy consumption, chemical inputs, and carbon emissions. Sequential precipitation strategies for phosphorus recovery, such as struvite and calcium phosphate formation, hold promise for producing reusable fertilizers. However, high operational costs and energy-intensive steps may hinder their scalability and environmental viability, including prolonged aeration, mechanical mixing, and pH adjustment through chemical dosing. Aeration alone accounts for 40–60% of energy consumption in conventional plants, while mechanical flocculation requires substantial power inputs, typically 0.5–2.0 kW·h/m³ (Liu, 2011). Meanwhile, chemical usage, particularly HCl for pH adjustment, further compounds operational expenses and emissions, with acid production alone emitting ~1.8 kg CO_2 per ton HCl due to its energy-intensive synthesis from chlorine and hydrogen gas (Misenheimer, 1986). These factors underscore the need for process optimization that targets both reaction kinetics and chemical dosing to achieve a sustainable, cost-effective recovery system.

Central to this optimization is the role of carbonate chemistry in CaP recovery. A critical yet underexplored factor in CaP recovery is the interplay between pH-dependent carbonate speciation after acidification of collected permeate and phosphate precipitation. As the Bjerrum plot illustrates, carbonate species partition dynamically with pH: at pH 6, aqueous CO_2 and HCO_3^- exist in near-equimolar concentrations, while CO2 becomes dominant below pH 6. Bicarbonate (HCO_3^-) actively competes with phosphate (PO_4^{3-}) for calcium (Ca^{2+}), favoring the formation of thermodynamically stable calcite ($CaCO_3$) over CaP—a reaction further exacerbated by the kinetic preference for $CaCO_3$ nucleation (Ren, 2021). This competition

manifests in recovered solids as residual calcite, diluting P content and reducing product purity. While acidic conditions (pH < 6) convert carbonate species to CO_2 (removable via aeration), partial acidification to intermediate pH levels (e.g., 6.5) leaves residual HCO_3^-, perpetuating $CaCO_3$ interference. Testing pH thresholds (4.5–6.5) thus aims to identify the optimal balance: pH 4.5 ensures complete CO_2 stripping but demands excessive acid, whereas pH 6.5 minimizes chemical use but risks significant $CaCO_3$ co-precipitation. By quantifying these trade-offs, we target a point where HCO_3^- interference is mitigated without overburdening the process with acid consumption.

These chemical interactions directly influence process efficiency and energy demands. Reducing the aeration time, minimizing the duration of mixing phases, and using lower chemical doses for pH adjustment could offer dual benefits: improving the economic feasibility of phosphorus recovery systems and lowering their carbon footprint. Research by Chai et al. (2015) demonstrated that optimizing these steps, especially aeration, can drastically improve the overall carbon efficiency of wastewater treatment systems. Similarly, Shen et al. (2023) emphasize that predictive control and better timing of chemical additions can reduce emissions and costs without compromising treatment performance.

This chapter focuses on two synergistic optimization objectives to enhance the sustainability and scalability of sequential phosphorus recovery:

1. Minimizing flocculation energy demand through kinetically tracking reactive phosphorus removal after CaO/$MgCl_2$ dosing. We aim to identify the minimum effective mixing time required for complete P agglomeration. Reducing mixing time to this range could cut

energy use by 30–50%, while simultaneously lowering wear on mechanical components—a critical advantage for full-scale implementation.

2. Acidification for carbonate removal currently relies on excessive HCl dosing (pH <4.5). By acidifying the collected permeate between a range of pH (4.5–6.5), we can target the threshold acidification level where residual bicarbonate (HCO_3^-) no longer inhibits CaP formation while minimizing calcite in recovery products.

Together, these optimizations address the core bottlenecks of sequential precipitation: energy-intensive mixing and chemical-dependent pH control. By coupling kinetic insights with carbonate chemistry, this work provides actionable strategies to reduce operational costs, energy demand, and emissions—key steps toward economically viable nutrient-scale nutrient recovery.

4.2 Materials and Methods

4.2.1 Kinetic Study of CaP Followed by Struvite Precipitation

The procedure outlined in Section 3.2.3.1 was modified to incorporate time-resolved sampling for reactive phosphorus (RP) to characterize the reaction kinetics of the sequential phosphorus recovery process. After adding CaO to the modified permeate, RP concentrations were measured at four intervals: 0.5, 1, 3, and 7 hours. This same time-course sampling approach was also applied during the subsequent struvite precipitation phase, following $MgCl_2$ addition. Preliminary trials indicated that most RP removal occurred within the first several hours, rendering the originally planned 24-hour sampling period unnecessary.

4.2.2 Modified Permeate Acidification Experiment

Four one-liter batches of modified permeate were adjusted to target pH values of 4.5, 5.0, 6.0, and 6.5 using 4 M hydrochloric acid (HCl). Each batch was then aerated for one hour at a flow rate of 0.5 L/min, replacing the previous 24-hour stirring-based degassing approach. To

evaluate CO_2 removal efficiency, alkalinity measurements were taken at three stages: before acidification, after pH adjustment, and after aeration.

After pretreatment, calcium oxide (CaO) was dosed into each beaker at a Ca: P molar ratio of 1:1. Reactive phosphorus (RP) was then monitored over time using the same kinetic sampling protocol described in Section 4.2.1.

4.2.3 Analytical Methods

Reactive phosphorus concentrations were measured at each recovery stage (post-struvite and post-calcium phosphate precipitation) to determine removal efficiencies. Immediately after sampling, solutions were filtered through sterile 0.45 μm polyethersulfone (PES) syringe filters (Thermo Scientific™ Nalgene™, Cat. No. 194-0045) to exclude suspended precipitates that could artificially elevate readings. The filtered permeate samples were then analyzed using TNT 845 (2–20 mg/L-P) test kits, selected based on expected concentration ranges. Absorbance was measured at 880 nm on a HACH DR 3900 spectrophotometer. Duplicate measurements were performed for each sample, with relative standard deviations (RSD) maintained below 5%.

4.3 Results and Discussion

4.3.1 Sequential Precipitation Kinetics: Calcium Phosphate to Struvite

The results of the kinetic trial using CaO followed by $MgCl_2$ addition are shown in Figures 4.1 and 4.4. The initial reactive phosphorus (RP) concentration was 82.2 mg/L PO_4^{3-}-P, with an alkalinity of 180 mg/L as $CaCO_3$ after overnight stirring—representing a 94% reduction in initial alkalinity due to prior pretreatment. Figure 4.1 illustrates the phosphorus removal efficiency over time at three Ca:P molar ratios (0.5:1, 1:1, and 2:1). The results indicate that phosphorus removal by CaO occurred rapidly across all doses, with the most substantial gains observed within the first hour of reaction. At a 2:1 Ca:P ratio, phosphorus removal reached

approximately 90% within 0.5 hours and plateaued by 3 hours, indicating near-complete precipitation. The 1:1 Ca:P ratio achieved around 75% removal by 7 hours, while the lowest dose (0.5:1) exhibited slower kinetics, plateauing near 60%. These results suggest diminishing returns in extending mixing time beyond 1–3 hours, particularly at higher Ca:P ratios, where reaction equilibrium is reached rapidly.

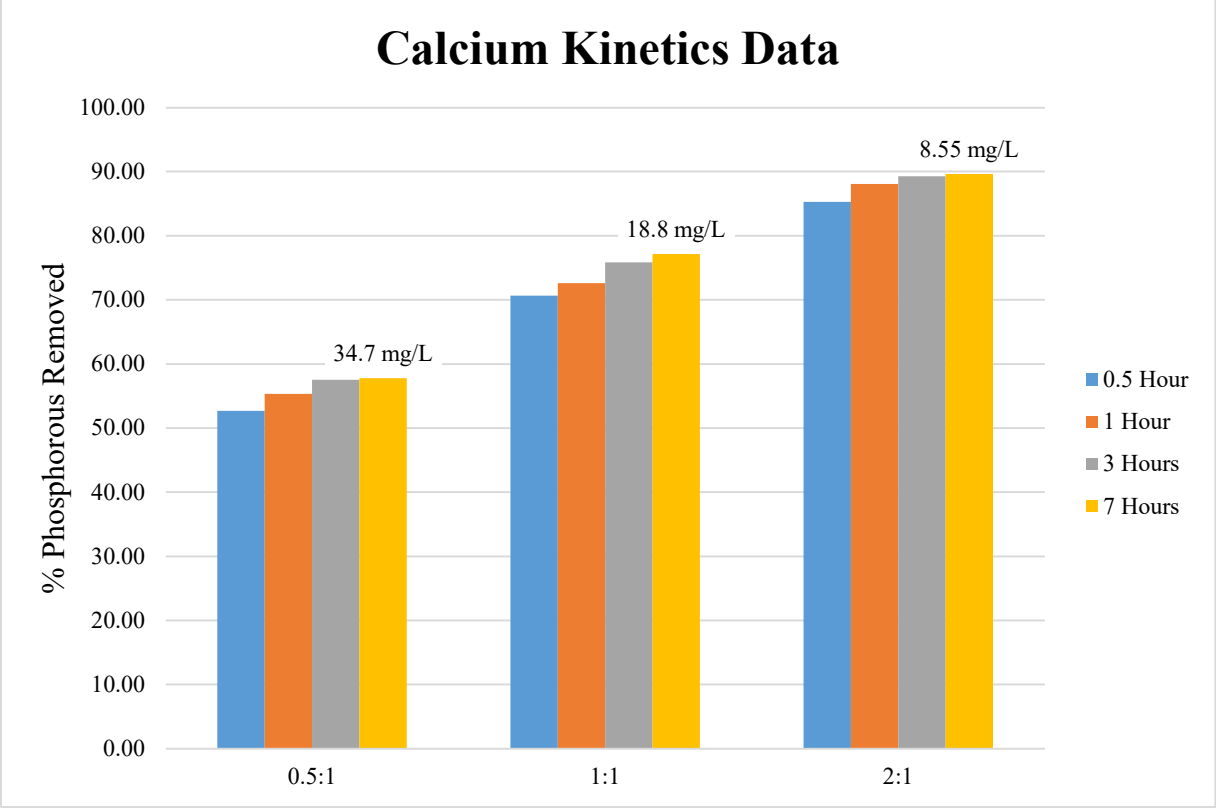

Figure 4.1: Kinetics of phosphorus removal following CaO addition in Trial 1 at Ca:P ratios of 0.5:1, 1:1, and 2:1. The initial PO_4^{3-}-P concentration was 72.8 mg/L Samples were analyzed at 0.5, 1, 3, and 7 hours to assess reaction progression. Removal rates increased modestly over time, with most of the removal occurring within the first hour.

In contrast, the magnesium precipitation phase (Figure 4.2) produced irregular trends. At the 0.5:1 Mg: P ratio, a gradual increase in phosphorus removal was observed over time, reaching an additional 36% removal, from the remaining measurable P after CaO addion, after 7 hours. However, for 1:1 and 2:1 Mg:P doses, initial measurements indicated negative removal

values, particularly within the first 0.5 to 1 hour, suggesting an apparent increase in measured RP concentration.

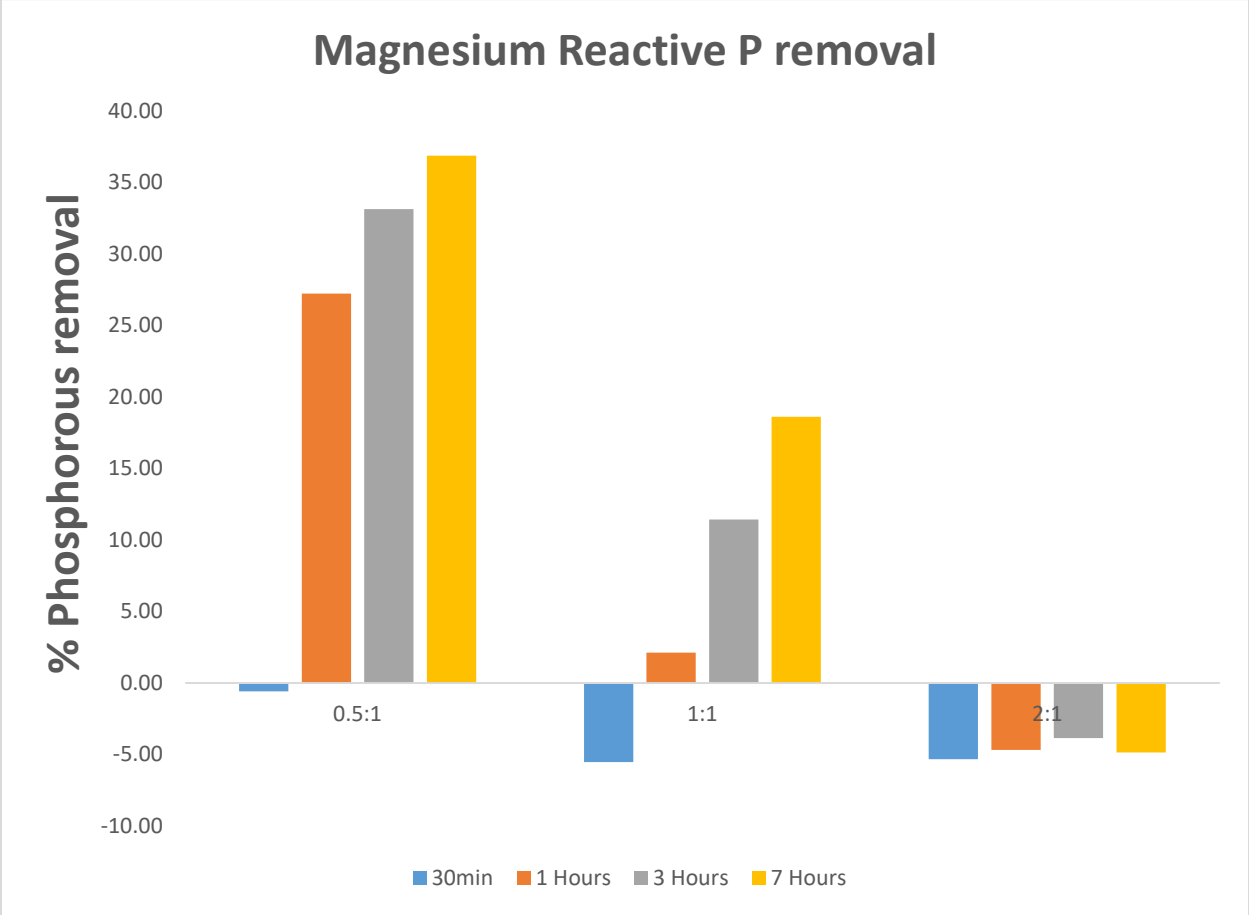

Figure 4.2: **Time-based phosphorus removal following $MgCl_2$ addition at different Mg:P molar ratios (0.5:1, 1:1, and 2:1) after prior CaO dosing.**

This unexpected increase may be attributed to partially redissolution of previously formed calcium phosphate before the $MgCl_2$ addition phase. While research suggests that CaP exhibits low solubility in water at pH 8, the observed RP release may result from complex interactions in the matrix or analytical variability due to colloidal solids (Wagner, 2022). However, without substantial evidence for significant Ca:P redissolution under these conditions, it is assumed that the negative values represent no additional RP removal during those times.

Overall, the kinetic data supports the conclusion that CaO is the dominant contributor to phosphorus removal in this sequential process. At higher Ca:P doses (1:1 and 2:1), RP removal was nearly complete after CaO addition, with little to no further removal observed during the struvite formation phase. These findings confirm that when Ca:P dosing is sufficient, the contribution of $MgCl_2$ to further RP reduction is minimal or negligible. Conversely, at lower Ca:P doses (e.g., 0.5:1), some additional phosphorus removal was achieved through struvite formation, but the overall efficiency was still lower than that of higher Ca:P conditions.

These kinetics highlight a critical trade-off: while CaO dosing at 2:1 achieves rapid and near-complete P removal, it also implies higher chemical use. Therefore, identifying the minimal Ca:P ratio that still achieves sufficient removal—ideally around 1:1—may represent a more cost-effective and sustainable operational target, especially if paired with optimized Mg dosing to capture residual P in low-Ca treatments.

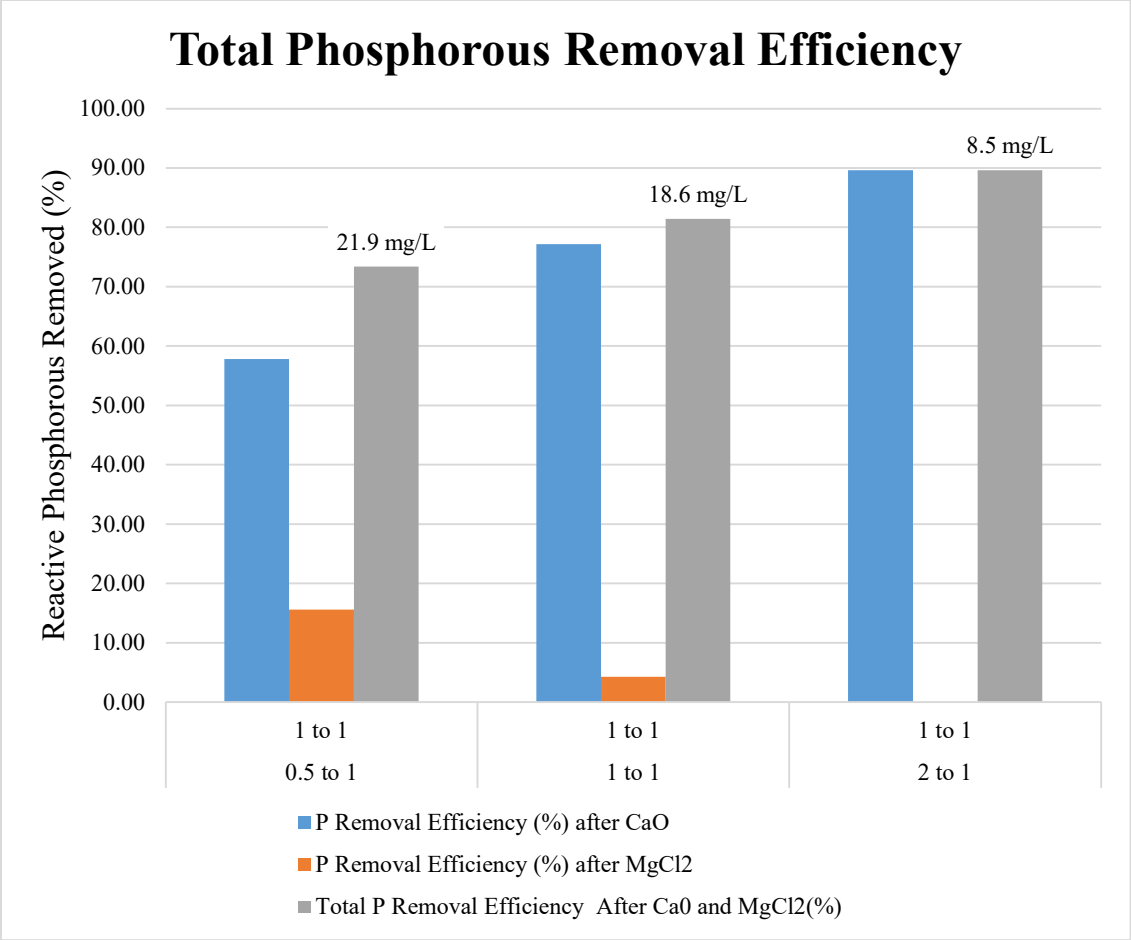

Figure 4.3: Total phosphorus removal efficiency after sequential chemical precipitation using CaO followed by $MgCl_2$ in Trial 1. Ca:P ratios ranged from 0.5:1 to 2:1, followed by a fixed Mg:P dose of 1:1. Highest combined removal (90%) was achieved at the 2:1 Ca:P condition, with an effluent P concentration of 8.5 mg/L

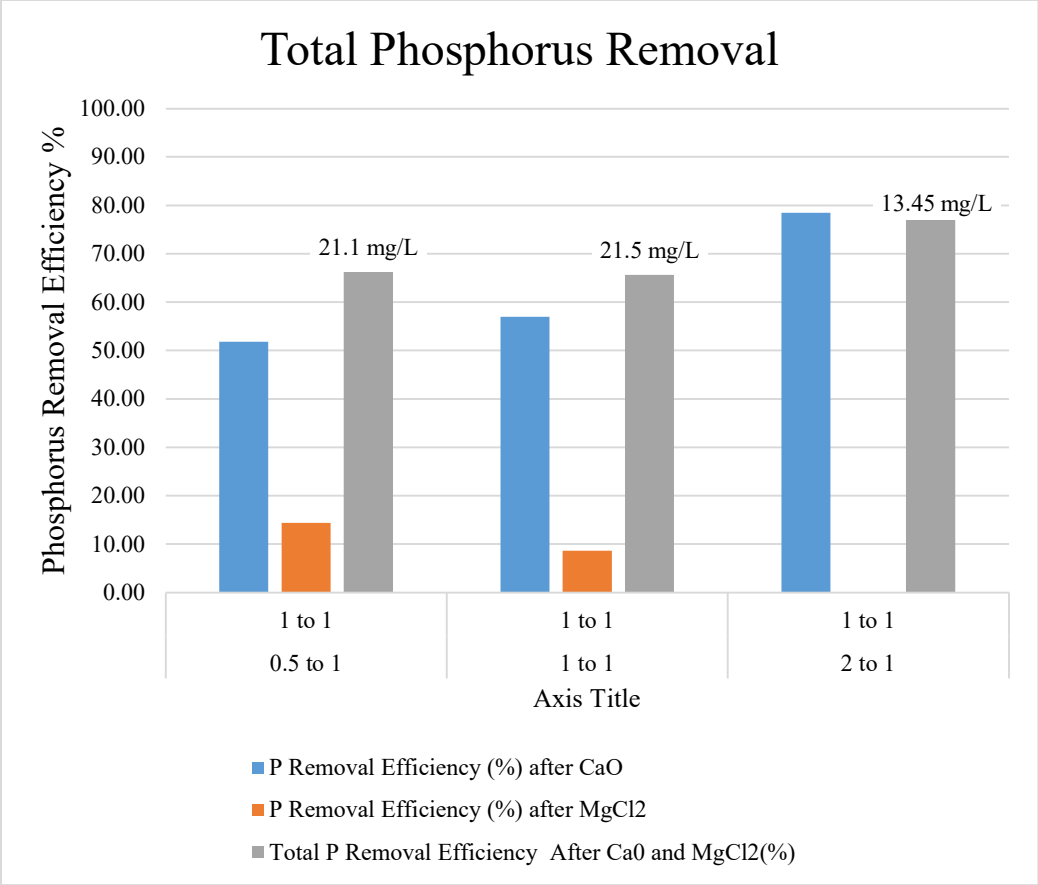

Figure 4.4: Total phosphorus removal during the sequential CaO followed by $MgCl_2$ addition in Trial 2, with an initial reactive phosphorus concentration of 62.5 mg/L. Blue bars represent P removal after CaO addition, orange bars show additional removal from $MgCl_2$, and green bars indicate cumulative removal.

The phosphorus removal trends observed following CaO addition were consistent across multiple independent trials. Replicate experiments conducted at Ca:P molar ratios of 0.5:1, 1:1, and 2:1 showed similar removal efficiencies and kinetic behaviors, with deviations typically within ±10% of the values reported in this trial based on the initial RP. In all cases, the majority of RP removal occurred within the first hour of CaO dosing, confirming the rapid kinetics and repeatability of calcium phosphate precipitation under the tested conditions. This reproducibility strengthens confidence in the use of CaO as a reliable primary precipitant for phosphorus recovery and supports its potential scalability in sequential treatment systems.

4.3.1.1 XRD Characterization Following Kinetic Trials

Reaction time significantly influenced both the removal efficiency and phase composition of the recovered calcium phosphate (CaP) products. In trial 1 of the kinetic testing, solids were harvested after only 7 hours of reaction time—considerably shorter than the 24–25 hours used in previous experiments detailed in Chapter 3. This abbreviated timeframe yielded notably different phase profiles, particularly at the 1:1 Ca:P ratio, where XRD analysis showed a product more dominated by hydroxyapatite (HAP), in contrast to the near-pure octacalcium phosphate (OCP) observed under extended reaction conditions.

At the lowest Ca:P ratio of 0.5:1, phosphorus removal was limited (~51%), and the recovered product exhibited broader XRD peaks with indications of mixed-phase composition, including HAP and minor calcite ($CaCO_3$). The presence of calcite suggests partial precipitation of calcium as carbonate, likely due to residual alkalinity in the permeate even after acidification. The early formation of HAP under these conditions suggests that even small calcium additions can drive crystallization of low-solubility P products, although with limited efficiency.

At a 1:1 Ca:P ratio, the product shifted toward a more crystalline hydroxyapatite phase—contrary to the 24-hour trial, where the same dose yielded over 99% OCP. This shift in mineralogy is likely attributed to kinetics: the shorter reaction period may not allow enough time for metastable OCP to dominate, instead favoring the formation of thermodynamically stable HAP at early stages of precipitation. This result emphasizes retention time's importance in governing product composition and potential solubility.

Together, these results underscore the tunability of the CaO-driven phosphorus recovery system. The shorter reaction period in Trial 2 reduced processing time and revealed how kinetic factors influence P removal efficiency and product composition. While high Ca:P ratios

consistently yielded effective removal, the choice of dose and reaction time can be optimized to produce CaP materials with tailored solubility, favoring amorphous, fast-release OCP at longer durations or crystalline, slow-release HAP at shorter time frames.

4.3.2 Effect of Permeate Acidification on P Recovery

Two independent trials evaluated the effect of initial acidification on alkalinity removal, pH, and chemical dosing requirements. In both trials, four batches of permeate were adjusted to pH targets of 4.5, 5.0, 6.0, and 6.5 using 4 M HCl, followed by one hour of aeration at 0.5 L/min.

In Trial 1, the initial alkalinity was 3980 mg/L as $CaCO_3$, and the initial reactive phosphorus (RP) concentration was 70.5 mg/L. Post-acidification alkalinity was entirely reduced to 0 mg/L at pH 4.5, while higher pH targets left residual alkalinity of 165 mg/L (pH 5), 1610 mg/L (pH 6), and 2730 mg/L (pH 6.5). After aeration, a very slight increase in alkalinity was observed, with values increasing to 50, 170, 1650, and 2575 mg/L, respectively. In Trial 2, the starting alkalinity was higher (4780 mg/L), and RP concentration was 73 mg/L. The pattern of alkalinity removal was consistent with Trial 1, with acidification to pH 4.5 again reducing alkalinity to zero, while progressively higher residuals were observed at increasing pH values. Post-aeration alkalinity increased slightly at pH 4.5 and 5.0, and more significantly at 6.0 and 6.5, reaching up to 3960 mg/L at the highest pH.

Alkalinity removal efficiency directly correlated with both the acid dose and target pH. As shown in Figure 4.5, partial removal of alkalinity was observed at intermediate pH values above pH 4.5. Interestingly, the volume of HCl required to reach each target pH varied significantly between trials and pH levels. For instance, reaching pH 4.5 required 13.0 mL and 22.9 mL of 4 M HCl in Trial 1 and Trial 2, respectively—a reflection of differing initial

buffering capacity and carbonate concentrations. This nonlinear chemical demand illustrates a potential cost bottleneck when full alkalinity removal is prioritized via strong acidification.

The observed increase in pH following aeration is primarily could be attributed to the removal of dissolved carbon dioxide (CO_2) from the permeate, which shifts the carbonate equilibrium toward lower hydrogen ion (H^+) concentrations. In aqueous solutions, CO_2 dissolves to form carbonic acid (H_2CO_3), which then dissociates into bicarbonate (HCO_3^-) and hydrogen ions, contributing to acidity. However, when CO_2 is stripped through aeration, this equilibrium is disrupted, leading to a decrease in H_2CO_3 and subsequent reduction in free H^+ ions, increasing the pH (Stumm and Morgan, 1996). This behavior is well-documented in water treatment systems where CO_2 removal via air stripping or aeration is used to raise pH without chemical addition (Metcalf & Eddy, 2014).

Additionally, the degree of pH adjustment is influenced by the buffering capacity of the permeate, which is governed by the concentrations of carbonate species (HCO_3^- and CO_3^{2-}). At higher initial alkalinities, as seen in Trial 2, the system exhibits stronger buffering and therefore a more pronounced pH rise upon CO_2 degassing. According to Tchobanoglous et al. (2003), this effect is especially significant in systems that undergo partial acidification, where sufficient bicarbonate remains to rapidly rebalance once CO_2 is removed.

Importantly, this natural pH elevation minimizes the need for chemical pH correction post-aeration and has direct benefits for CaP precipitation, which occurs optimally in the pH range of 7 to 9.5 (Linyu Deng and Bipro Ranjan Dhar, 2023). These findings reinforce the strategic value of aeration not just for CO_2 removal, but also as an efficient method for achieving the target pH range for phosphate recovery without reliance on additional chemical dosing.

4.3.2.1 P Removal Efficiency

Phosphorus (P) removal following acidification and aeration was partially influenced by the initial pH adjustment and residual alkalinity. Across both trials, a clear kinetic trend emerged in which P removal improved with longer reaction time and, in most cases, with decreasing pH. However, optimal performance did not occur at the most acidic condition (pH 4.5), but instead in the intermediate range (pH 6.0–6.5).

In Trial 1, initial P removal was lowest at pH 5.0, reaching only 42% after 1 hour and 55% after 7 hours (Figure 4.5). Acidification to pH 4.5 performed slightly better but still underperformed compared to higher pH levels, plateauing at 67% removal. By contrast, the most effective removal occurred at pH 6.0, which reached 76% after 7 hours. pH 6.5 also demonstrated high performance (76% at 7 hours), despite higher residual alkalinity.

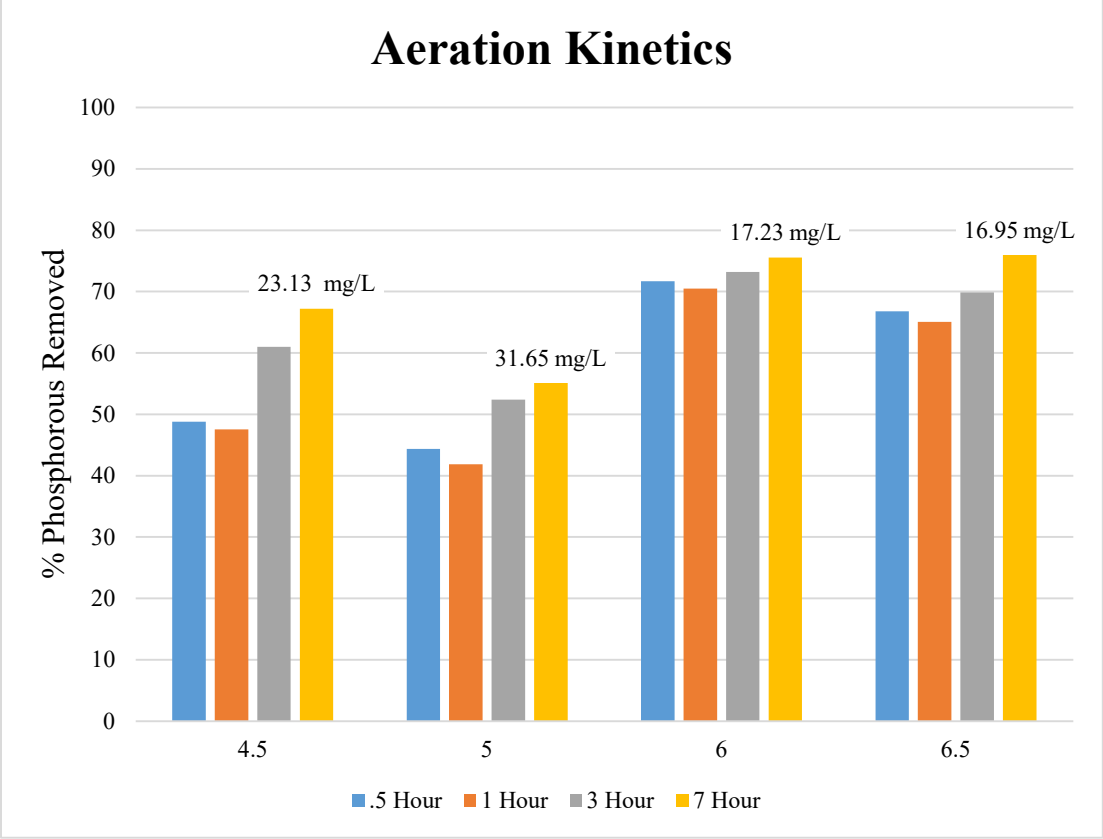

Figure 4.5: Trial 1 of phosphorus removal after varying pH pretreatment methods, followed by one hour of aeration. Phosphorus removal efficiencies at initial pH values of 4.5, 5, 6, and 6.5 following 0.5, 1, 3, and 7 hours of aeration.

In Trial 2, the results were consistent but showed slightly higher removal across all pH conditions, which could likely be due to the higher initial P. Again, pH 6.0 and 6.5 yielded the highest removal at 77% and 74%, respectively, after 7 hours. Interestingly, pH 5.0 also showed strong performance in this trial, reaching 74% by 7 hours—potentially due to more effective CO_2 stripping during aeration as indicated by the larger pH rebound in this condition post aeration. Acidification to pH 4.5 again performed the worst, reaching only 63% after 7 hours, even though it had the lowest post-aeration alkalinity.

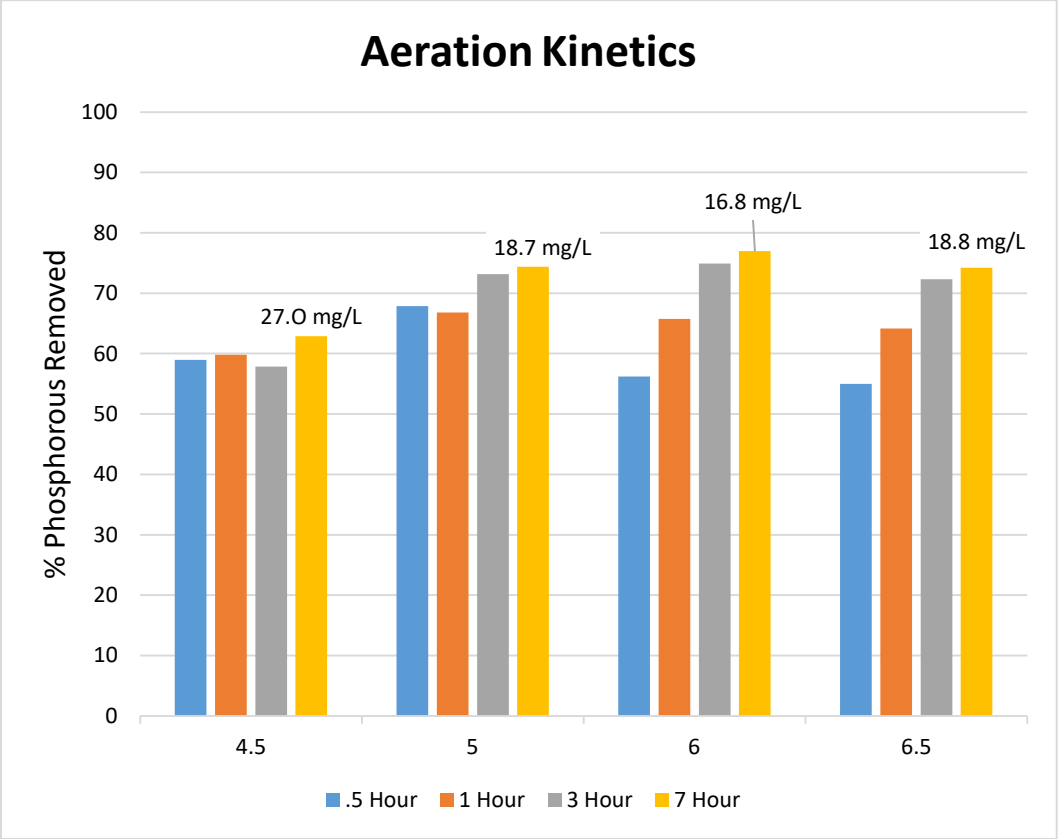

Figure 4.6: Replicated phosphorus removal results across pH 4.5 to 6.5, showing similar trends to Trial 1. Maximum removal was again achieved at pH 6 after 7 hours of aeration, yielding an effluent concentration of 16.8 mg/L. Across both trials, aeration times of 3–7 hours significantly enhanced performance, confirming the importance of carbonate stripping prior to calcium addition for optimal CaP recovery.

These results confirm that extreme acidification to pH 4.5 is not necessary and may, in fact, hinder phosphorus removal. While this condition achieves near-complete carbonate removal, the excess acidity may interfere with early-stage CaP nucleation or shift the equilibrium away from favorable precipitation conditions. In contrast, pH values of 6.0–6.5 align closely with literature-reported optimal ranges for CaP formation (pH 7.0–9.5) and benefit from natural pH rebound during aeration, which returned the solution to a favorable precipitation environment without further chemical adjustment. The consistent high performance at these intermediate pH values highlights the importance of targeting efficient acidification rather than complete carbonate stripping.

Taken together, the data suggest that moderate acidification to pH 5.5–6.0 offers the most reliable and cost-effective path forward, achieving high phosphorus removal efficiency while minimizing chemical inputs and supporting process scalability. These findings further validate the coupling of short aeration periods with partial acidification as a viable strategy for enhancing CaP recovery without extensive energy or reagent demand.

4.5 Discussions and Conclusions

This study investigated two synergistic strategies for improving the sustainability and efficiency of phosphorus recovery through sequential calcium phosphate (CaP) and struvite precipitation: (1) minimizing mixing time through kinetic profiling of phosphorus removal, and (2) reducing chemical inputs via controlled acidification and aeration of permeate to enhance carbonate removal. Together, these strategies address process bottlenecks that would lead to high energy demands and excessive chemical dosing, possibly affecting the scalability of nutrient recovery systems.

The kinetic trials confirmed that CaO addition alone could account for the majority of reactive phosphorus (RP) removal, with efficiencies reaching upwards of 90% within the first hour at a Ca:P ratio of 2:1. Increasing the Ca:P ratio consistently improved both the speed and completeness of removal, but with diminishing returns beyond 1:1. In contrast, the contribution of struvite formation via $MgCl_2$ addition was minimal when Ca:P dosing was sufficient, suggesting that the secondary magnesium stage functions more effectively as a polishing step in low-Ca systems. These results align with prior studies that emphasize the rapid kinetics of CaP nucleation and the competitive interaction between phosphate and carbonate species for calcium ions.

The total phosphorus removal data reinforced this conclusion: combined removal efficiencies increased with Ca:P ratio, but the benefit of $MgCl_2$ dosing declined sharply as more phosphorus was removed in the initial CaP step. At a Ca:P ratio of 2:1, nearly complete phosphorus removal was achieved through CaO alone. In contrast, lower Ca:P ratios (e.g., 0.5:1) relied more heavily on the magnesium stage to achieve acceptable overall performance. Importantly, these results were highly reproducible across trials, with minimal variation in removal kinetics and plateau values, reinforcing the reliability and scalability of CaO dosing for phosphorus capture.

Parallel trials on permeate acidification revealed how carbonate speciation and pH dynamics influence the CaP precipitation process. While complete carbonate removal was achieved through acidification to pH 4.5, this condition consistently produced lower P removal efficiencies than intermediate pH values. Excess acidity may disrupt early CaP nucleation, reduce calcium ion activity, or lower the saturation index for CaP formation. In contrast, pH 6.0 or 6.5 acidification yielded the highest phosphorus removal in both trials, despite leaving

significant residual alkalinity. These pH levels strike a balance by partially removing inhibitory bicarbonate while retaining conditions favorable for CaP formation, especially when combined with a one-hour aeration step.

Crucially, aeration enabled pH rebound into the optimal range (7.0–9.5) for CaP precipitation without further chemical adjustment. This behavior, driven by CO_2 stripping and carbonate re-equilibration, allowed the system to self-correct toward favorable precipitation conditions, reducing the need for post-aeration base addition. The pH rose so effectively in some cases that HCl had to be added to bring the system back down to 8.2–8.5. These findings support the use of aeration not only for CO_2 removal but also as a strategic process tool for passive pH adjustment, lowering both chemical and energy requirements.

Chapter 5 - Summary and Future Recommendations

During these experiments and the work that predated me, the groundwork was laid to show the feasibility of sequential phosphorus removal in producing useful fertilizer products in the form of calcium phosphate and struvite. This thesis also expands the scope of nutrient recovery by demonstrating ammonia adsorption and desorption using clinoptilolite, offering additional pathways for resource recovery in wastewater systems.

In Chapter 2, a predictive modeling tool was developed to simulate ammonia adsorption and desorption in three clinoptilolite-packed columns operated in series. Experimental breakthrough data were collected from a column trial using anaerobic membrane bioreactors (AnMBR) permeate with an influent ammonia concentration of approximately 860 mg/L. The model enabled precise operation of the system by predicting saturation points and minimizing effluent ammonia concentrations, which were successfully kept below 20 mg/L throughout much of the column operation. Following saturation, a 0.5 M NaCl brine solution was used to desorb the ammonia from the zeolite beds, and desorption curves were modeled to inform regeneration strategies.

Chapter 3 validated the sequential phosphorus recovery concept by showing that CO_2 stripping and acidification of high-alkalinity effluent enhances the precipitation of calcium phosphate. The remaining phosphorus was then successfully recovered as struvite through magnesium addition and pH elevation.

Chapter 4 built upon this by optimizing operational variables including aeration strategy, acidification timing, and magnesium dosing. The results supported the idea that sequential recovery not only improves total phosphorus removal but also results in two distinct fertilizer products with potential agronomic value.

These findings contribute to the growing body of research that positions nutrient recovery as a sustainable and resource-generating alternative to conventional wastewater treatment. The tools, models, and experiments presented here form a basis for future work toward scalable, closed-loop nutrient recovery systems.

The work presented in this thesis demonstrates the feasibility of integrated nutrient recovery through both phosphorus and nitrogen capture using calcium phosphate precipitation, struvite formation, and clinoptilolite adsorption. However, several important areas remain for future research and system refinement:

1. **Improvement of Rapid Mixing in Scaled-Up CaP Recovery**

   Initial 35-liter-scale trials of calcium phosphate precipitation demonstrated >70% phosphorus removal using a 2:1 Ca:P molar ratio, confirming the potential for larger-scale operation. However, the rapid mixing phase in the current basin configuration has limitations in achieving a uniform distribution of the coagulant and consistent floc formation. Future research should focus on optimizing the hydraulics and mixing energy in this step to improve solid-liquid separation efficiency and precipitation kinetics.

2. **Scaled-Up Sequential Recovery of CaP and Struvite**

   While laboratory-scale sequential recovery of CaP followed by struvite has shown promise, this process has not yet been tested at scale using the current treatment basin. The decanting and separating solids between the two steps may present operational challenges, particularly regarding avoiding re-dissolution or mixing precipitates. Design modifications or staged separation strategies may be necessary to maintain high product quality and recovery efficiency.

3. **Characterization of Combined Phosphorus and Nitrogen Removal**

   Preliminary results suggest that sequential phosphorus and nitrogen removal is feasible using a combination of the scaled-up CaP precipitation basin and zeolite-packed columns. However, a more comprehensive characterization of this integrated process is needed. This includes mass balance analyses, nutrient speciation, and effluent quality assessment to quantify the removal efficiencies and better understand the interactions between the two stages.

4. **Assessment of Clinoptilolite Performance Over Multiple Cycles**

   The repeated use of clinoptilolite for ammonia adsorption and brine-based desorption introduces long-term performance and material fatigue questions. Future studies should evaluate the adsorption capacity, regeneration efficiency, and structural integrity of the zeolite after multiple cycles in column operation. This will inform the media's expected service life and its economic feasibility for reuse.

5. **Continuation of Ammonium Sulfate Recovery via Desorption**

   Continue previous work, further research is recommended to optimize the recovery of ammonium sulfate as a usable fertilizer product from the desorption solution. This includes improving the efficiency of ammonia desorption, understanding the purity of the recovered product, and evaluating its potential agronomic applications.

These research directions aim to build on the foundation established in this thesis and move the technology closer to real-world implementation. Continued progress in these areas will support the development of scalable, integrated nutrient recovery systems that are both environmentally and economically sustainable.

References

(1) Hedström, A.; Amofah, L. R. Adsorption and Desorption of Ammonium by Clinoptilolite Adsorbent in Municipal Wastewater Treatment Systems. Journal of Environmental Engineering & Science 2008, 7 (1), 53–61. https://doi.org/10.1139/S07-029.

(2) Damodara Kannan, A.; Parameswaran, P. Ammonia Adsorption and Recovery from Swine Wastewater Permeate Using Naturally Occurring Clinoptilolite. Journal of Water Process Engineering 2021, 43, 102234. https://doi.org/10.1016/j.jwpe.2021.102234.

(3) Huang, H.; Xiao, X.; Yan, B.; Yang, L. Ammonium Removal from Aqueous Solutions by Using Natural Chinese (Chende) Zeolite as Adsorbent. Journal of Hazardous Materials 2010, 175 (1), 247–252. https://doi.org/10.1016/j.jhazmat.2009.09.156.

(4) Martins, T. H.; Souza, T. S. O.; Foresti, E. Ammonium Removal from Landfill Leachate by Clinoptilolite Adsorption Followed by Bioregeneration. Journal of Environmental Chemical Engineering 2017, 5 (1), 63–68. https://doi.org/10.1016/j.jece.2016.11.024.

(5) Reiss, A. G.; Wang, X.; Ye, Y.; Kan, A. T.; Tomson, M. B. An Experimental and Modeling Study of CaCO3 Nucleation and Inhibition by PAPEMP under a Regime of Increasing Oversaturation with Implications for Crystallization and Scale Formation. Applied Geochemistry 2025, 183, 106322. https://doi.org/10.1016/j.apgeochem.2025.106322.

(6) Avdeef, Alex.; Kearney, D. L.; Brown, J. A.; Chemotti, A. R. Bjerrum Plots for the Determination of Systematic Concentration Errors in Titration Data. Anal. Chem. 1982, 54 (13), 2322–2326. https://doi.org/10.1021/ac00250a041.

(7) Ramirez-Gil, J. G.; Lopera, A. A.; Garcia, C. Calcium Phosphate Nanoparticles Improve Growth Parameters and Mitigate Stress Associated with Climatic Variability in Avocado Fruit. Heliyon 2023, 9 (8), e18658. https://doi.org/10.1016/j.heliyon.2023.e18658.

(8) Amjad, Z. Calcium Phosphates in Biological and Industrial Systems; Springer Science & Business Media, 2013.

(9) Calcium-Modified Clinoptilolite as a Recovery Medium of Phosphate and Potassium from Anaerobically Digested Olive Mill Wastewater | Request PDF. ResearchGate 2025. https://doi.org/10.1007/s11356-019-07212-5.

(10) Wellmer, F.-W.; Scholz, R. W.; Bastian, D. Can Ultimate Recoverable Resources (URRs) Be Assessed? Does Analyzing Declining Ore Grades Help? Miner Econ 2023, 36 (4), 599–613. https://doi.org/10.1007/s13563-023-00368-0.

(11) Cities and a circular economy for food. https://www.ellenmacarthurfoundation.org/cities-and-a-circular-economy-for-food/overview (accessed 2025-04-15).

(12) Han, R.; Wang, Y.; Zou, W.; Wang, Y.; Shi, J. Comparison of Linear and Nonlinear Analysis in Estimating the Thomas Model Parameters for Methylene Blue Adsorption onto Natural Zeolite in Fixed-Bed Column. Journal of Hazardous Materials 2007, 145 (1), 331–335. https://doi.org/10.1016/j.jhazmat.2006.12.027.

(13) Weatherley, L. R.; Miladinovic, N. D. Comparison of the Ion Exchange Uptake of Ammonium Ion onto New Zealand Clinoptilolite and Mordenite. Water Res 2004, 38 (20), 4305–4312. https://doi.org/10.1016/j.watres.2004.08.026.

(14) Document Display | NEPIS | US EPA. https://nepis.epa.gov/Exe/ZyNET.exe/2000TNHN.TXT?ZyActionD=ZyDocument&Client=EPA&Index=1981+Thru+1985&Docs=&Query=&Time=&EndTime=&SearchMethod=1&TocRestrict=n&Toc=&TocEntry=&QField=&QFieldYear=&QFieldMonth=&QFieldDay=&IntQFieldOp=0&ExtQFieldOp=0&XmlQuery=&File=D%3A%5Czyfiles%5CIndex%20Data%5C81thru85%5CTxt%5C00000010%5C2000TNHN.txt&User=ANONYMOUS&Password=anonymous&SortMethod=h%7C-&MaximumDocuments=1&FuzzyDegree=0&ImageQuality=r75g8/r75g8/x150y150g16/i425&Display=hpfr&DefSeekPage=x&SearchBack=ZyActionL&Back=ZyActionS&BackDesc=Results%20page&MaximumPages=1&ZyEntry=1&SeekPage=x&ZyPURL (accessed 2025-04-15).

(15) Kim, D.; Min, K. J.; Lee, K.; Yu, M. S.; Park, K. Y. Effects of pH, Molar Ratios and Pre-Treatment on Phosphorus Recovery through Struvite Crystallization from Effluent of Anaerobically Digested Swine Wastewater. Environmental Engineering Research 2017, 22 (1), 12–18. https://doi.org/10.4491/eer.2016.037.

(16) Shao, X.; Huang, Y.; Wood, R. M.; Tarpeh, W. A. Electrochemical Sulfate Production from Sulfide-Containing Wastewaters and Integration.

(17) Ritchie, H.; Rosado, P.; Roser, M. Environmental Impacts of Food Production. Our World in Data 2022.

(18) Ritchie, H.; Rosado, P.; Roser, M. Environmental Impacts of Food Production. Our World in Data 2022.

(19) US EPA, O. Estimated Animal Agriculture Nitrogen and Phosphorus from Manure. https://www.epa.gov/nutrientpollution/estimated-animal-agriculture-nitrogen-and-phosphorus-manure (accessed 2025-03-19).

(20) Walling, E.; Vaneeckhaute, C. Greenhouse Gas Emissions from Inorganic and Organic Fertilizer Production and Use: A Review of Emission Factors and Their Variability. Journal of Environmental Management 2020, 276, 111211. https://doi.org/10.1016/j.jenvman.2020.111211.

(21) Gulf of Mexico 'dead zone' larger than average, scientists find | National Oceanic and Atmospheric Administration. https://www.noaa.gov/news-release/gulf-of-mexico-dead-zone-larger-than-average-scientists-find (accessed 2025-04-15).

(22) Impacts of Waste from Concentrated Animal Feeding Operations on Water Quality. https://doi.org/10.1289/ehp.8839.

(23) Mallin, M. A.; Cahoon, L. B. Industrialized Animal Production—A Major Source of Nutrient and Microbial Pollution to Aquatic Ecosystems. Population and Environment 2003, 24 (5), 369–385. https://doi.org/10.1023/A:1023690824045.

(24) Mallin, M. A.; Cahoon, L. B. Industrialized Animal Production—A Major Source of Nutrient and Microbial Pollution to Aquatic Ecosystems. Population and Environment 2003, 24 (5), 369–385. https://doi.org/10.1023/A:1023690824045.

(25) Faulconer, E. K.; Mazyck, D. W. Influence of Activated Carbon Surface Oxygen Functionality on Elemental Mercury Adsorption from Aqueous Solution. Journal of Environmental Chemical Engineering 2017, 5 (3), 2879–2885. https://doi.org/10.1016/j.jece.2017.05.036.

(26) Vasquez, M. M.; Tyson, K. J.; Hawkins, B. T.; Trotochaud, L. Integration of Silicate Minerals for Ammonium and Phosphate Removal with an On-Site Wastewater Treatment Prototype. PLOS Water 2022, 1 (9), e0000048. https://doi.org/10.1371/journal.pwat.0000048.

(27) Wang, Y.; Lin, F.; Pang, W. Ion Exchange of Ammonium in Natural and Synthesized Zeolites. Journal of Hazardous Materials 2008, 160 (2), 371–375. https://doi.org/10.1016/j.jhazmat.2008.03.006.

(28) Razon, L. F. Life Cycle Analysis of an Alternative to the Haber-Bosch Process: Non-Renewable Energy Usage and Global Warming Potential of Liquid Ammonia from Cyanobacteria. Environmental Progress & Sustainable Energy 2014, 33 (2), 618–624. https://doi.org/10.1002/ep.11817.

(29) Managing Manure Nutrients at Concentrated Animal Feeding Operations.

(30) Manyi-Loh, C. E.; Mamphweli, S. N.; Meyer, E. L.; Okoh, A. I.; Makaka, G.; Simon, M. Microbial Anaerobic Digestion (Bio-Digesters) as an Approach to the Decontamination of Animal Wastes in Pollution Control and the Generation of Renewable Energy. Int J Environ Res Public Health 2013, 10 (9), 4390–4417. https://doi.org/10.3390/ijerph10094390.

(31) Mostaghaci, B.; Hanifi, A.; Loretz, B.; Lehr, C.-M. Nano-Particulate Calcium Phosphate as a Gene Delivery System. In Non-Viral Gene Therapy; Yuan, X., Ed.; InTech, 2011. https://doi.org/10.5772/18948.

(32) National Water Quality Inventory: Report to Congress.

(33) Wang, S.; Peng, Y. Natural Zeolites as Effective Adsorbents in Water and Wastewater Treatment. Chemical Engineering Journal 2010, 156 (1), 11–24. https://doi.org/10.1016/j.cej.2009.10.029.

(34) Eberle, S.; Schmalz, V.; Börnick, H.; Stolte, S. Natural Zeolites for the Sorption of Ammonium: Breakthrough Curve Evaluation and Modeling. Molecules 2023, 28 (4), 1614. https://doi.org/10.3390/molecules28041614.

(35) Casson, J. P.; Olson, B. M.; Little, J. L.; Nolan, S. C. Nitrogen Loss in Surface Runoff.

(36) US EPA, O. Nonpoint Source: Agriculture. https://www.epa.gov/nps/nonpoint-source-agriculture (accessed 2025-04-15).

(37) Nutrient recovery from wastewater and reuse in agriculture: a review | Request PDF. https://www.researchgate.net/publication/348450773_Nutrient_recovery_from_wastewater_and_reuse_in_agriculture_a_review (accessed 2025-04-15).

(38) Maurer, M.; Schwegler, P.; Larsen, T. A. Nutrients in Urine: Energetic Aspects of Removal and Recovery. Water Science and Technology 2003, 48 (1), 37–46. https://doi.org/10.2166/wst.2003.0011.

(39) Bai, Z.; Liu, L.; Kroeze, C.; Strokal, M.; Chen, X.; Yuan, Z.; Ma, L. Optimizing Phosphorus Fertilizer Use to Enhance Water Quality, Food Security and Social Equality. Resources,

Conservation and Recycling 2024, 203, 107400. https://doi.org/10.1016/j.resconrec.2023.107400.

(40) (PDF) Phosphorous in the Environment: Characteristics with Distribution and Effects, Removal Mechanisms, Treatment Technologies, and Factors Affecting Recovery as Minerals in Natural and Engineered Systems. ResearchGate 2024. https://doi.org/10.1007/s11356-019-04732-y.

(41) (PDF) Pigs, Profits, and Rural Communities. ResearchGate 2024. https://doi.org/10.2307/2654412.

(42) (PDF) Struvite precipitation with MgO as a precursor: Application to wastewater treatment. https://www.researchgate.net/publication/276930086_Struvite_precipitation_with_MgO_as_a_precursor_Application_to_wastewater_treatment?utm_source=chatgpt.com (accessed 2025-04-15).

(43) (PDF) The Quest for Sustainable Nitrogen Removal Technologies. ResearchGate 2024. https://doi.org/10.2166/wst.2003.0018.

(44) Performance of secondary P-fertilizers in pot experiments analyzed by phosphorus X-ray absorption near-edge structure (XANES) spectroscopy | Ambio. https://link.springer.com/article/10.1007/s13280-017-0973-z (accessed 2025-04-15).

(45) Ren, C.; Li, Y.; Zhou, Q.; Li, W. Phosphate Uptake by Calcite: Constraints of Concentration and pH on the Formation of Calcium Phosphate Precipitates. Chemical Geology 2021, 579, 120365. https://doi.org/10.1016/j.chemgeo.2021.120365.

(46) Phosphates and Ammonia Recovery from Secondary Effluents by Selective Ion Exchange with Production of a Slow-Release Fertilizer. Water Research 1979, 13 (1), 65–73. https://doi.org/10.1016/0043-1354(79)90256-2.

(47) Deng, L.; Dhar, B. R. Phosphorus Recovery from Wastewater via Calcium Phosphate Precipitation: A Critical Review of Methods, Progress, and Insights. Chemosphere 2023, 330, 138685. https://doi.org/10.1016/j.chemosphere.2023.138685.

(48) Preparation and evaluation of zeolites for ammonium removal from municipal wastewater through ion exchange process | Scientific Reports. https://www.nature.com/articles/s41598-020-69348-6?utm_source=chatgpt.com (accessed 2025-04-15).

(49) Bian, Z.; Tian, H.; Yang, Q.; Xu, R.; Pan, S.; Zhang, B. Production and Application of Manure Nitrogen and Phosphorus in the United States since 1860. Earth System Science Data 2021, 13 (2), 515–527. https://doi.org/10.5194/essd-13-515-2021.

(50) Wasielewski, S.; Rott, E.; Minke, R.; Steinmetz, H. Recovery of Ammonium Sulfate Solution by Regeneration of Loaded Clinoptilolite. Nanomaterials (Basel) 2022, 12 (3), 525. https://doi.org/10.3390/nano12030525.

(51) Kocatürk-Schumacher, N. P.; Zwart, K.; Bruun, S.; Stoumann Jensen, L.; Sørensen, H.; Brussaard, L. Recovery of Nutrients from the Liquid Fraction of Digestate: Use of Enriched Zeolite and Biochar as Nitrogen Fertilizers. Journal of Plant Nutrition and Soil Science 2019, 182 (2), 187–195. https://doi.org/10.1002/jpln.201800271.

(52) Türker, M.; Çelen, I. Removal of Ammonia as Struvite from Anaerobic Digester Effluents and Recycling of Magnesium and Phosphate. Bioresource Technology 2007, 98 (8), 1529–1534. https://doi.org/10.1016/j.biortech.2006.06.026.

(53) Kang, X.; Csetenyi, L.; Gao, X.; Gadd, G. M. Solubilization of Struvite and Biorecovery of Cerium by Aspergillus Niger. Appl Microbiol Biotechnol 2022, 106 (2), 821–833. https://doi.org/10.1007/s00253-021-11721-0.

(54) David, M. B.; Drinkwater, L. E.; McIsaac, G. F. Sources of Nitrate Yields in the Mississippi River Basin. Journal of Environmental Quality 2010, 39 (5), 1657–1667. https://doi.org/10.2134/jeq2010.0115.

(55) Avramenko, M.; Nakashima, K.; Kawasaki, S. State-of-the-Art Review on Engineering Uses of Calcium Phosphate Compounds: An Eco-Friendly Approach for Soil Improvement. Materials 2022, 15 (19), 6878. https://doi.org/10.3390/ma15196878.

(56) Struvite Precipitation in Anaerobic Swine Lagoon Liquid: Effect of pH and Mg:P Ratio and Determination of Rate Constant | Request PDF. ResearchGate 2024. https://doi.org/10.1016/S0960-8524(03)00076-2.

(57) Bansiwal, A. K.; Rayalu, S. S.; Labhasetwar, N. K.; Juwarkar, A. A.; Devotta, S. Surfactant-Modified Zeolite as a Slow Release Fertilizer for Phosphorus. J. Agric. Food Chem. 2006, 54 (13), 4773–4779. https://doi.org/10.1021/jf060034b.

(58) Surfactant-Modified Zeolite as a Slow Release Fertilizer for Phosphorus | Request PDF. ResearchGate 2024. https://doi.org/10.1021/jf060034b.

(59) Scholz, R. W.; Wellmer, F.-W.; Mew, M.; Steiner, G. The Dynamics of Increasing Mineral Resources and Improving Resource Efficiency: Prospects for Mid- and Long-Term Security of Phosphorus Supply. Resources, Conservation and Recycling 2025, 213, 107993. https://doi.org/10.1016/j.resconrec.2024.107993.

(60) Liu, C.; Li, S.; Zhang, F. The Oxygen Transfer Efficiency and Economic Cost Analysis of Aeration System in Municipal Wastewater Treatment Plant. Energy Procedia 2011, 5, 2437–2443. https://doi.org/10.1016/j.egypro.2011.03.419.

(61) The Use of Zeolites as an Addition to Fertilisers – A Review. CATENA 2022, 213, 106125. https://doi.org/10.1016/j.catena.2022.106125.

(62) Wang_Natural zealots as effective absorbents.pdf. Google Docs. https://drive.google.com/file/d/1QAVTW88y0jhupBtI7jJ0B0vNms3Pqjke/view?usp=embed_facebook (accessed 2025-04-15).

(63) Wastewater Technology Fact Sheet: Package Plants.

(64) Kotoulas, A.; Agathou, D.; Triantaphyllidou, I. E.; Tatoulis, T. I.; Akratos, C. S.; Tekerlekopoulou, A. G.; Vayenas, D. V. Zeolite as a Potential Medium for Ammonium Recovery and Second Cheese Whey Treatment. Water 2019, 11 (1), 136. https://doi.org/10.3390/w11010136.

Appendix A

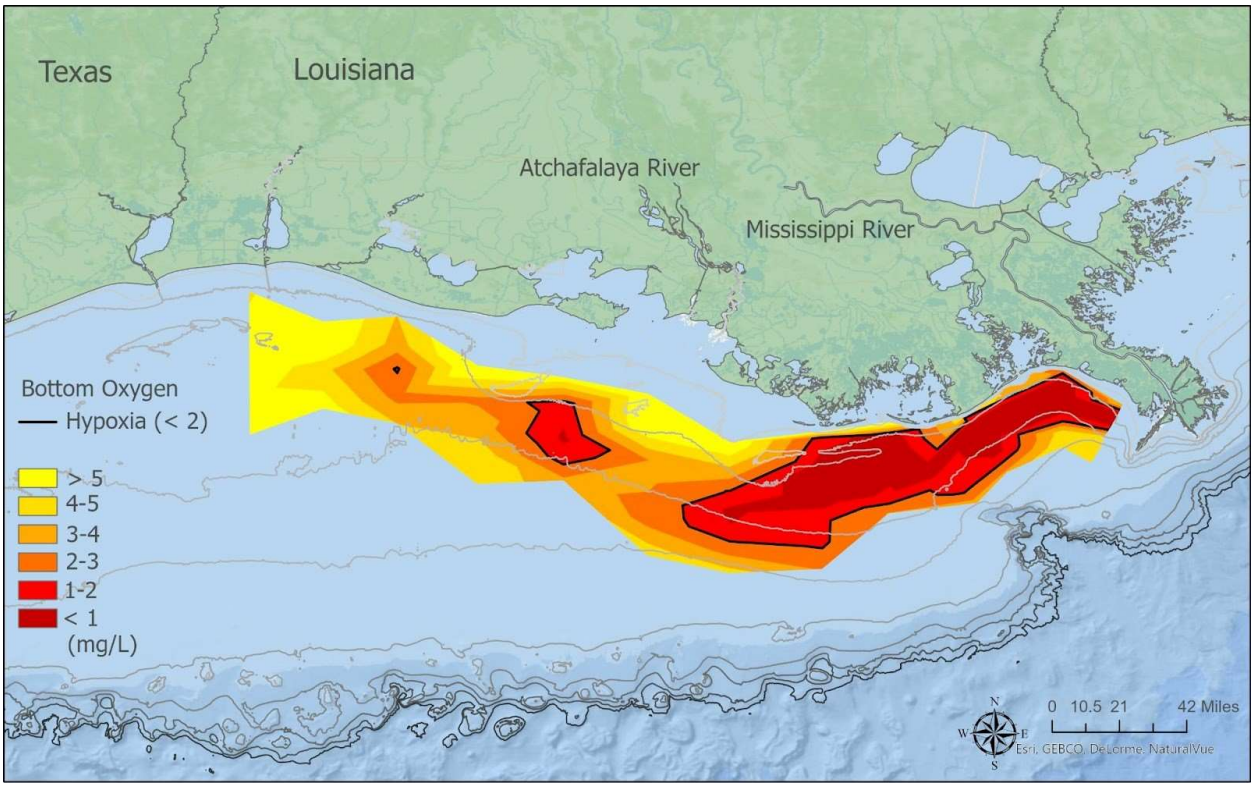

Error! No text of specified style in document. **Figure A.1: NOAA map depicting the 2024 Gulf of Mexico hypoxic zone (commonly referred to as the "dead zone"),**

Appendix B

Component	XRF Results %
SiO	67
Al_2O_3	10.7
CaO	1.52
MgO	0.47
Na_2O	2.55
K_2O	3.65
Fe_2O_3	0.96
MnO	0.03

Table B.2: XRF analysis results showing the composition (%) of clinoptilolite used in this study.

Parameter	Permeate (Range)	Permeate (Avg)
pH	7.19–7.65	7.42
Turbidity (TU)	0.27–0.61	0.52
TCOD (mg/L)	223–742	515
BOD (mg/L)	43.0–197	767
Phosphorus (mg/L)	41.2–118	79.6
Ammonia (mg/L)	369–1468	918.5

Table B.3: Physicochemical characteristics of anaerobic membrane bioreactor (AnMBR) permeate used.

	Column 1			Column 2			Column 3		
Time (Hr)	NH3-N Adsorbed (g)	C/Co	Effluent Concentration (mg/L)	NH3-N Adsorbed (g)	C/Co	Effluent Concentration (mg/L)	NH3-N Adsorbed (g)	C/Co	Effluent Concentration (mg/L)
0	0	0	0	0	0	0	0	0	0
1	0.6804	0	0	0	0	0	0	0	0
2	1.3608	0	0	0	0	0	0	0	0
3	2.0412	0.176780895	200.4695355	0	0	0	0	0	0
4	2.7216	0.510998121	579.4718691	0.347683121	0	0	0	0	0
5	3.402	1	1134	1.3608	0	0	0	0	0
6	3.5	1	1134	2.0412	0.176781	200.4695355	0	0	0
7	3.5	1	1134	2.7216	0.510998	579.4718691	0.347683121	0	0
8	3.5	1	1134	3.402	1	1134	1.3608	0	0
9	3.5	1	1134	3.5	1	1134	2.0412	0.176781	1.767808955
10	3.5	1	1134	3.5	1	1134	2.7216	0.510998	5.109981209

Figure B.2: Predictive modeling of NH_4^+-N adsorption in a three-column clinoptilolite system using breakthrough curve simulations.

Appendix C

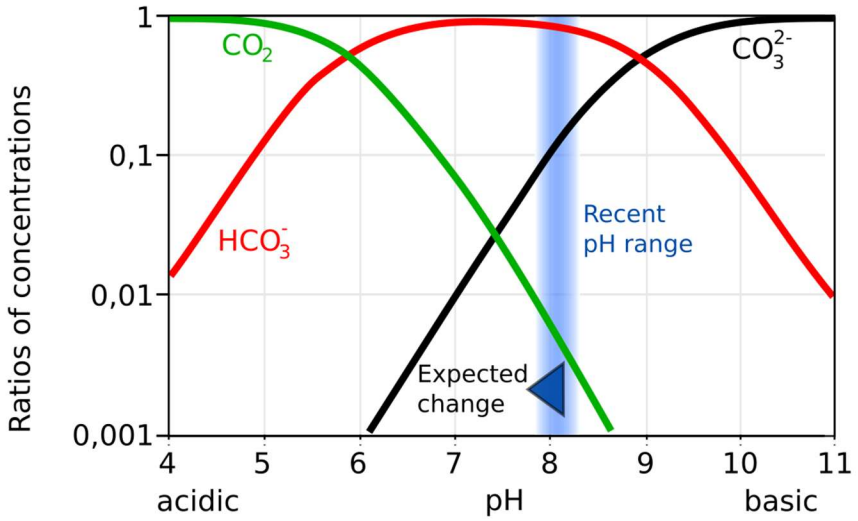

Figure C.3: Bjerrum plot showing the distribution of inorganic carbon species (CO_2, HCO_3^-, and CO_3^{2-}) as a function of pH in aqueous systems.

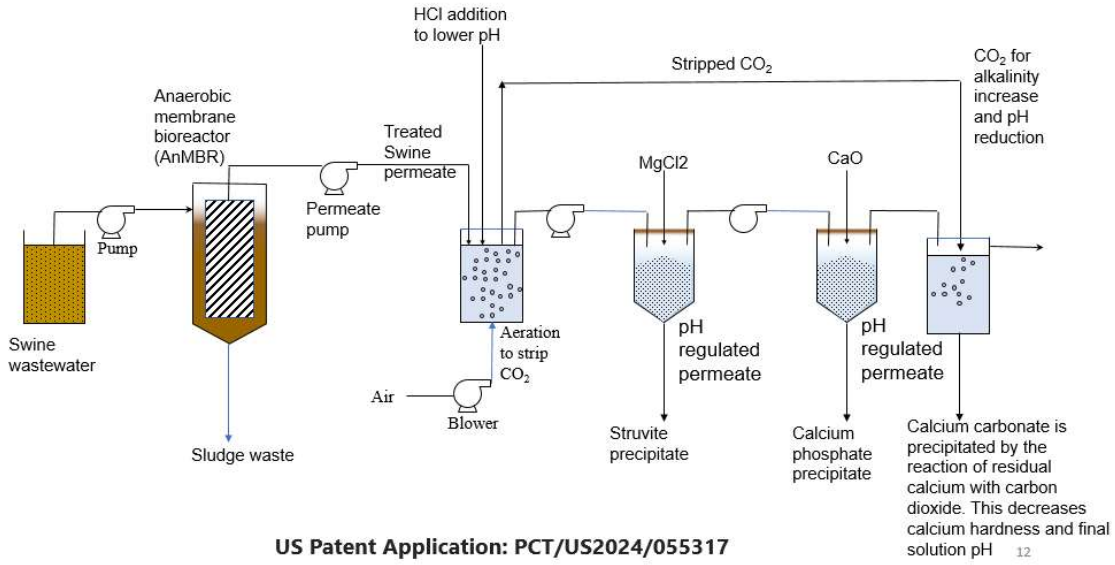

Figure C.4: Process schematic of a sequential nutrient recovery system for swine wastewater treatment, adapted from US Patent Application PCT/US2024/055317.